

Spread of a non-Newtonian liquid jet over a horizontal plate

JIANGANG ZHAO AND ROGER E. KHAYAT

Department of Mechanical and Materials Engineering, The University of Western Ontario, London,
Ontario, Canada N6A 5B9
rkhayat@uwo.ca

(Received 2 March 2007 and in revised form 29 June 2008)

The flow of an impinging non-Newtonian jet onto a solid flat plate is examined theoretically in this study. Similarity solutions are sought for both shear-thinning and shear-thickening fluids of the power-law type. The jet is assumed to spread out in a thin layer bounded by a hydraulic jump. In addition to the stagnation-flow region, the flow domain is divided into three main regions: a developing boundary layer, fully viscous boundary layer and hydraulic jump. The anomalous behaviour of power-law fluids at small shear rate is remedied by seeking a two-layer solution in each domain. Such anomalies include the singularity of viscosity for shear-thinning fluids, and the vanishing of viscosity as well the overshoot in velocity for shear-thickening fluids. Although the rate of shear-thinning appears to affect significantly the film profile and velocity, only the overall viscosity influences the position of the hydraulic jump.

1. Introduction

This study focuses on the analysis of the two-dimensional thin-film flow formed when a free laminar jet of a non-Newtonian fluid impinges vertically onto and spreads over a horizontal plate. The liquid spreads in a thin layer until the depth increases, suddenly forming a hydraulic jump. The problem thus consists of obtaining the shape of the free surface, the flow field within the film and the jump position. Both shear-thinning and shear-thickening fluids will be considered. Although the impinging jet of Newtonian fluids has been extensively investigated in the literature, little work has been devoted to the impingement of a non-Newtonian jet.

The impingement of a Newtonian jet was considered by Watson (1964), who examined both the radial and planar jet spread for steady laminar and turbulent flows. Neglecting surface-tension effects and using a thin-film or boundary-layer approach, Watson found that for a two-dimensional jet at impinging velocity U_0 , the steady jet surface height (in units of half jet width (a)) grows at a rate equal to $1.81/Re_N$, where $Re_N = aU_0/\nu$ is the Reynolds number, with ν being the kinematic viscosity. A relation between the jump location and height was also obtained for both laminar and turbulent flows. Watson's theory was tested in a number of experimental investigations, including those of Watson himself, Craik *et al.* (1981), Stevens & Webb (1992), Bush & Aristoff (2003) and Baonga, Louahlia-Gualous & Imbert (2006). In particular, Watson's theoretical predictions for the free-surface velocity and film thickness were experimentally verified by Stevens & Webb (1992) and Baonga *et al.* (2006). In an effort to improve Watson's theory, Bush & Aristoff (2003) included the influence of surface tension for small radius circular jumps, leading to better

agreement with experiment. It is, however, generally agreed that Watson's theory is adequate for circular jumps with large radius and height (see § 7 for further discussion).

For an impinging non-Newtonian jet, few studies are available. Kashkarov & Mikhaelyan (1973) considered the problem of a two-dimensional laminar power-law jet striking normally on a horizontal plate. However, they simply established a relation between the velocity distribution and the rheological properties of the fluid. Gorla (1977) extended the similarity solution of Watson (1964) to laminar swirling power-law jet, and obtained the expressions for the free-surface radial velocity, growth of the free surface and skin friction coefficient.

As the boundary layer develops from the stagnation region, it gradually absorbs the whole of the flow until the viscous forces reach the free surface and the spreading jet is in the fully viscous boundary-layer region in the form of thin-film flow. Thin-film flow, in turn, has been extensively investigated in the literature. The influence of inertia, gravity and substrate topography on the steady flow and early stages of flow development of Newtonian and non-Newtonian thin films was previously examined by Khayat and co-workers. In particular, in their work on Newtonian coating flow, Khayat & Welke (2001) used Watson's similarity solution (1964) for steady film surface to assess the validity of their nonlinear formulation. Kim & Khayat (2002) used a spectral method to obtain the solution for power-law fluid flowing on a horizontal surface during early development. Khayat & Kim (2006) examined the interplay between inertia and elasticity during the steady and transient coating flow of an Oldroyd-B fluid.

A closely related problem to non-Newtonian jet spread flow is the boundary-layer flow of non-Newtonian fluid, which has been the subject of theoretical and numerical investigations. Early studies were conducted by Schowalter (1960), and Acrivos, Shah & Petersen (1960), who considered the boundary-layer equations for a power-law fluid. Schowalter (1960) demonstrated that similarity solutions are possible provided the external velocity, $U(x)$, behaves like x^m , where x is the coordinate along the surface of the body. The particular case $m=0$, which corresponds to the flow past a flat plate, was solved by Acrivos *et al.* (1960). Similarity solutions for a power-law fluid flow past a right-angle wedge ($m=1/3$) and along a wedge with opening angle $2\pi/3$ ($m=1/2$) were provided by Lee & Ames (1966) and Andersson & Irgens (1988), respectively. Experimental studies of non-Newtonian boundary-layer flow are less common. For Newtonian fluids, the boundary-layer assumption is valid at large Reynolds number; the boundary-layer equations are obtained from the Navier–Stokes equations by neglecting higher-order terms in the inverse of the Reynolds number. In contrast, for shear-thinning fluids, the boundary-layer equations remain accurate even when the Reynolds number is not large (Wu & Thompson 1996). This is probably attributable to the high shearing in the boundary-layer region, with inertia still expected to be dominant.

Although the power-law model often fits rheological data well over certain stress ranges, and has the benefit of analytic simplicity, it is valid only in regions above a certain minimum shear rate. Near a free surface or edge of the boundary layer where the shear rate tends to zero, the effective viscosity tends to infinity for shear-thinning fluids, and zero for shear-thickening fluids. Despite this fundamental shortcoming, the power-law model is frequently used in studies of boundary-layer flow and free-surface flow (Acrivos *et al.* 1960; Andersson & Irgens 1988; Weinstein, Ruschak & Ng 2003). Although no pronounced side effects are reported from using the power-law model, some curious physical behaviour was nevertheless reported. Acrivos *et al.* (1960) found that for shear-thickening fluids, the boundary layer terminates at a

finite distance (on the boundary-layer length scale) from the solid plate. According to Denier & Dabrowski (2004), this observation indicates a physically unrealistic overshoot of the streamwise velocity for boundary-layer flow (that is, a region in which the streamwise velocity exceeds the velocity in the outer potential flow). For shear-thinning fluids, Denier & Dabrowski (2004) also alluded to the difficulty in the case of an algebraically decaying velocity field with regards to matching such a solution to an inviscid outer (potential) flow. The possibility of such matching is implicitly assumed in the boundary-layer approximation. They also pointed to the parallel between this algebraic decay and that for Newtonian fluids; general similarity solutions, leading to the Falkner–Skan similarity equation, possess algebraically decaying behaviour.

The conditions for successful matching of these solutions onto an outer potential flow were examined by Brown & Stewartson (1965), who also discussed the relevance of similarity solutions to the asymptotic description of a real boundary layer. They demonstrated that solutions exhibiting algebraic decay are not appropriate if such solutions are to be matched onto an outer potential flow. However, the case here for the spread of a non-Newtonian jet is somewhat complicated by the simultaneous appearance of nonlinearities resulting from inertia, free surface and viscosity. The nonlinear terms in the apparent viscosity, which are typically neglected in boundary-layer theory, prove crucial in correctly describing the matching of the inner boundary layer with an outer potential flow. Denier & Dabrowski (2004) considered the problem of the boundary-layer flow of a power-law fluid and solved the boundary-layer equations in similarity form. For shear-thickening fluids, they provided a rigorous mathematical justification for the existence of a finite-width boundary layer, and introduced a secondary viscous adjustment layer to smooth out the solution and to ensure correct matching with the far-field boundary conditions. In the case of shear-thinning fluids, they showed that smooth matching between the inner algebraically decaying solutions and an outer uniform flow can be achieved via the introduction of a viscous diffusion layer.

The focus of the current study is on the interplay between inertia and non-Newtonian effects for thin-film flow. Watson's (1964) assumptions remain valid, particularly those of moderately large inertia effect and a jump occurring far from impingement. Consequently, surface tension effects will be neglected. The gravitational pressure gradient is similarly neglected except in the hydraulic jump region. In §2, the large-Reynolds-number limit of the conservation equations for a power-law fluid are established. These are shown to reduce to a modified form of the classical boundary-layer equations, with the inclusion of a nonlinear term to model the non-uniform vertical diffusion of viscosity. Section 3 considers the fully developed viscous boundary-layer region where a similarity solution is obtained. For both shear-thinning and shear-thickening fluids, a thin outer adjustment viscous layer is required near the free surface in order to smooth out the inner solution as the free surface is approached. Similarly, in §4 the numerical similarity solution is sought in the developing boundary-layer region, for both shear-thinning and shear-thickening fluids. It is demonstrated that a viscous adjustment layer is required in order to ensure a smooth asymptotic matching to the far-outer-field flow solution. In §5, the flow in the entire physical domain is obtained upon matching the flows between the developing and fully viscous boundary-layer regions. Section 6 considers an approximate solution for the developing boundary-layer region, and the corresponding approximate solution to the flow in the entire physical domain is obtained. In §7, the principle of momentum is applied at the hydraulic jump, and a relation is derived between the position and height of the jump. Finally, some concluding remarks are given in §8.

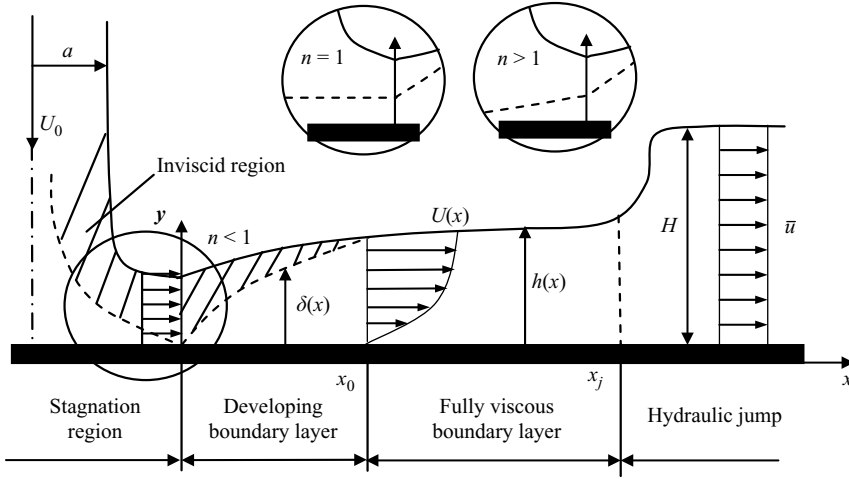


FIGURE 1. Schematic illustration of the symmetric plane jet flow impinging on a flat solid plate. Note that the flow variables are dimensionless.

2. Governing equations and boundary conditions

Consider the steady laminar incompressible flow of a planar jet of a non-Newtonian fluid of width $2a$ impinging at a (uniform) velocity U_0 on a fixed flat plate lying normally to the jet direction. The flow configuration is depicted schematically in figure 1. Only half of the physical domain is shown in the figure because of flow symmetry. In this work, starred variables are dimensional, and dimensionless variables will be introduced shortly (note that dimensionless variables are used in the figure for clarity). The x^* -axis is taken along the flat plate and the y^* -axis coincides with the jet axis. Following Watson (1964), four distinct regions of flow are identified for a power-law fluid, with smooth passage from one region to the next: the stagnation-flow region (i); the boundary-layer region (ii); the fully viscous thin-film region (iii). Under some flow conditions, a hydraulic jump may form in region (iv).

In the vicinity of the stagnation point, in region (i), $x^* = O(a)$ The speed outside the boundary layer rises rapidly from 0 at the stagnation point to the impingement velocity U_0 in the inviscid far region. For a Newtonian fluid, the boundary-layer thickness δ_N^* remains constant and is estimated in terms of the strength of the outside potential flow (see Schlichting 1979) as $\delta_N^* = O(\sqrt{\nu \dot{\epsilon}/U_0})$, where $\dot{\epsilon}$ is the rate of streamwise elongation of the potential flow. In contrast, for a power-law fluid, Sarweswar & Manohar (1968) showed that the boundary-layer thickness depends on position, and is written here as

$$\delta^* = \left[nm \left(\frac{\delta_N^{*2}}{5.76\nu} \right)^{2-n} x^{*(n-1)} \right]^{1/(n+1)},$$

where m and n are the consistency coefficient and power-law index, respectively. Although the boundary layer varies as $(x^*)^{(n-1)/(n+1)}$ in region (i), it grows as $(x^*)^{1/(n+1)}$ in region (ii), as will be shown in § 5. Thus, for shear-thinning fluids, the boundary-layer thickness exhibits a singularity at the stagnation point and decays algebraically with distance. Figure 1 depicts schematically the flow for shear-thinning fluids ($n < 1$) in the main figure, where δ^* is taken to decay to a negligible level between regions

(i) and (ii) before it begins to grow again. Also added, as insets, are the cases of a Newtonian ($n = 1$) and shear-thickening ($n > 1$) fluids in region (i). Thus, the constant boundary-layer thickness in region (i) for a Newtonian fluid grows as $\sqrt{x^*}$ far from the stagnation point in region (ii). That for shear-thickening fluids grows from zero in the stagnation-flow region at a smaller rate than in region (ii).

For greater values of x^* , in region (ii), the elongation rate weakens with distance, but the flow remains two-dimensional as a result of non-negligible surface curvature. The speed outside the boundary layer remains almost constant, equal to U_0 , as the fluid here is unaffected by the viscous stresses. If $x^* \gg a$, so that the flow in region (ii) is not affected by the stagnation flow in region (i), the flow can be determined by seeking a solution of the boundary-layer equations of the Blasius type. This region, $a \ll x^* < x_0^*$, will be referred to as the developing boundary-layer region, with boundary-layer thickness $\delta^*(x^*)$, outside which the flow is inviscid and constant. Here x_0^* is the location of the transition point at which viscous stresses become appreciable right up to the free surface where the whole flow is of the boundary-layer type. At this point, the velocity profile changes from the Blasius type to the similarity profile. The flow in region (iii), $x^* > x_0^*$, which will be referred to as the fully-developed boundary-layer region, is bounded by the flat plate and the free surface $y^* = h^*(x^*)$. Finally, the hydraulic jump in region (iv) is of height H^* and occurs at a location $x^* = x_j^*$, which can be larger or smaller than x_0^* since the jump may occur at any point in the flow.

In this work, the fluid is described by the Ostwald–de Waele power-law model (see, for instance, Bird, Stewart & Lightfoot 2002), and the excess stress tensor is given by

$$\tau^* = \mu^* \mathbf{D}^* \equiv m \left[\frac{1}{2} (\mathbf{D}^* : \mathbf{D}^*) \right]^{(n-1)/2} \mathbf{D}^*, \tag{2.1}$$

where $\mathbf{D}^* = \nabla^* \mathbf{v}^* + \nabla^{*t} \mathbf{v}^{*t}$ is the rate-of-strain tensor, with \mathbf{v}^* being the velocity vector, and t denotes matrix transposition. In this case, the viscosity μ^* is given explicitly by

$$\mu^* = m [2(u_x^*)^2 + 2(v_y^*)^2 + (u_y^* + v_x^*)^2]^{(n-1)/2}, \tag{2.2}$$

where u^* and v^* are the velocity components in the horizontal and vertical directions, respectively. Note that a subscript x or y denotes partial differentiation. The film thickness is assumed to be small everywhere, and the classical thin-film theory is assumed to hold. In this work, aRe and a are taken as length scales in the x and y directions, respectively, where $Re = \rho U_0^{2-n} a^n / m$ is the generalized Reynolds number for the jet flow. This expression suggests that the range of validity of the boundary-layer assumption may be limited to $n < 2$ (Acrivos *et al.* 1960). The boundary-layer thickness in region (i) is expressed in dimensionless form in terms of the Reynolds number and the boundary-layer thickness for the reference Newtonian flow as

$$\delta = \left[n \left(\frac{Re_N \delta_N^2}{5.76 Re} \right)^{2-n} x^{(n-1)} \right]^{1/(n+1)}.$$

The velocity scales in the x and y directions are taken as U_0 and U_0/Re , respectively. In this case, the dimensionless viscosity, μ , is given by

$$\mu = [u_y^2 + 2\varepsilon^2(u_y v_x + u_x^2 + v_y^2) + \varepsilon^4 v_x^2]^{(n-1)/2}, \tag{2.3}$$

where $\varepsilon = 1/Re$, and u and v are the dimensionless velocity components in the x and y directions, respectively. The non-dimensionalized conservation equations are written as

$$u_x + v_y = 0, \tag{2.4a}$$

$$uu_x + vu_y = 2\varepsilon^2(\mu u_x)_x + [\mu(u_y + \varepsilon^2 v_x)]_y. \quad (2.4b)$$

In this work, Re is assumed to be moderately large, and ε will be the small parameter in the problem. However, as will be seen later, higher-order terms appearing in (2.3) and (2.4) are not uniformly negligible. If only leading-order terms in ε are retained, the momentum equation (2.4b) for a thin jet reduces to:

$$uu_x + vu_y = (|u_y|^{n-1}u_y)_y. \quad (2.5)$$

At the plate, the no-slip and no-penetration conditions are assumed to hold, so that

$$u(x, 0) = v(x, 0) = 0. \quad (2.6)$$

The flow field is sought separately in the developing boundary-layer region ($x < x_0$), fully developed boundary-layer region ($x > x_0$), and hydraulic jump region. It is convenient to first examine the flow in the $x > x_0$ region.

3. Fully developed viscous boundary-layer flow ($x > x_0$)

Consider first the flow in the fully developed boundary-layer region (iii) or $x > x_0$. The present study is focused on film flow in the visco-inertial range. It is argued here that the surface-tension effect is negligible for two main reasons. First, the film is assumed to be thin. More importantly, the local curvature of the film free surface is assumed to be sufficiently small for the current boundary-layer approach to hold. Secondly, the surface-tension coefficient of typical polymeric fluids is small. Lee & Mei (1996) examined the formation of steady solitary waves on inclined Newtonian thin-film flow, and determined the dependence of the Weber number of different liquids on the Reynolds number for both small and large angles of inclination. They found that the surface-tension effect decreases strongly with inertia. Lee & Mei's results show that the capillary number, $Ca_N = \mu U_0 / \sigma$, for a Newtonian fluid of viscosity μ and surface tension σ , behaves roughly as $Ca_N \sim Re_N^2 / \varepsilon$. Here ε is the ratio of film thickness and length. This suggests that the effect of surface tension for a thin film is $O(\varepsilon^4 / Re_N^2)$. Note that the surface tension effect for thin-film flow is $O(\varepsilon^3 / Ca_N)$ (see Khayat & Kim 2006). Omodei (1979) carried out a two-dimensional finite-element simulation of steady Newtonian jet flow. He found that the height of the free surface changes by 8% when the capillary number changes from 0.83 to infinity at a Reynolds number (based on channel exit half-height) equal to 1, compared to a change in jet thickness of less than 1% when the Reynolds number is greater than 10. A further drop in capillary number is thus required to observe any palpable change in jet height at moderately large Reynolds number. However, further decrease in Ca_N is not realistic according to experiment. See, for instance, the early study by Goren & Wronski (1966) on capillary jet flow. The capillary number can be large even for some (essentially) Newtonian fluids with high viscosity such as polybutene oils. As an illustration, consider polybutene oil with mean viscosity, $\mu = 80$ mPa s, density $\rho = 1200$ kg m⁻³, and surface-tension coefficient $\sigma = 50$ mN m⁻¹. The film is assumed to move at 12 m s⁻¹ out of an annulus of 2 mm gap, on a cylindrical substrate of radius 20 mm. In this case, $\varepsilon = 0.1$, $Re_N = 36$ and $Ca_N = 19.2$, making a surface tension effect of $O(10^{-5})$. The surface-tension effect is expected to be even less significant for typical polymeric films because of higher viscosity and lower surface-tension coefficient. In polymer processing, such as the injection moulding of polybutene (see Behrens *et al.* 1987), the capillary number is $O(10-100)$. Polymer solution jets take generally longer to break up than Newtonian jets of comparable (shear) viscosity; polymeric jets may not form

droplets at all (Gordon, Yerushalmi & Shinnar 1973; Christanti & Walker 2002). Melt fracture occurs essentially in the absence of the surface-tension effect for elastic fluids. Even weakly elastic fluids can exhibit moderately large capillary numbers, such as 0.5 and 0.75% polyethylene oxides moving at a speed of 10 ms^{-1} , with capillary numbers equal to 1.2 and 11, respectively. Strongly elastic polyacrylamide solutions of 0.1 to 0.75% lead to corresponding capillary numbers in the range 16 to 600 (Middleman 1987). In order to illustrate the situation for shear-thinning and shear-thickening fluids, a generalized capillary number must be introduced, which can be written as $Ca = mU_0^n/a^{n-1}\sigma$. Since a is small, the surface-tension effect can be important for shear-thinning fluids relative to Newtonian fluids and especially relative to shear-thickening fluids. Even for shear-thinning fluids, however, surface tension is not expected to play a significant role for thin films. Referring to the data in figure 11, consider a jet of half width $a = 8\text{ mm}$, impinging at velocity $U_0 = 8\text{ ms}^{-1}$, with $m = 100\text{ Pa s}^n$ and $n = 0.2$. In this case, $Ca = 6.37$ for a fluid with $\sigma = 50\text{ mN m}^{-1}$, making the surface-tension effect, at most, $O(\varepsilon^3)$.

Let $U(x) \equiv u(x, y = h)$ and $V(x) \equiv v(x, y = h)$ denote the velocity components at the free surface. In the absence of surface tension, the kinematic and dynamic conditions can be written, respectively, as

$$V(x) = U(x)h'(x), \tag{3.1}$$

$$u_y(x, y = h) = 0, \tag{3.2}$$

where a prime denotes total differentiation. In this case, the following similarity solution can be used, namely

$$u(x, y) = U(x)f(\eta), \tag{3.3}$$

where $\eta = y/h(x)$ is the similarity variable. The following boundary conditions on f must be satisfied:

$$f(0) = 0, \quad f(1) = 1, \quad f'(1) = 0. \tag{3.4}$$

The constancy of the volume flux is expressed as

$$\int_0^{h(x)} u(x, y) dy = U(x)h(x) \int_0^1 f(\eta) d\eta = 1. \tag{3.5}$$

Hence, $U(x)h(x)$ is constant. Integrating (2.4a) and using the similarity solution (3.3) leads to

$$v(x, y) = h'(x)\eta f(\eta)U(x). \tag{3.6}$$

Note that (3.6) reduces to (3.1) at $y = h(x)$. Upon substituting u and v from (3.3) and (3.6), respectively, the equation of motion (2.5) reduces to

$$\frac{h^{n+1}}{nU^{n-1}}U' = f^{-2}(f')^{n-1}f'' = -\frac{3c^{n+1}}{n+1}, \tag{3.7}$$

where c is an unknown constant to be determined. For shear-thickening fluids ($n > 1$), the equation for f on the right-hand side of (3.7) becomes singular in the limit $\eta = 1$ when the third condition in (3.4) is imposed. However, although this singularity is

removable (see below), it reflects a physical anomaly as the viscosity vanishes at the free surface for shear-thickening fluids, and becomes infinite for shear-thinning fluids. An asymptotic solution is therefore required as the free surface is approached, and will be carried out shortly. Multiplying (3.7) by f' and integrating once with respect to η and using the third boundary condition in (3.4), gives

$$f' = c(1 - f^3)^{1/(n+1)}. \quad (3.8)$$

The unknown c is found upon integrating (3.8) over the interval $[0, 1]$ and using the condition $f(1) = 1$ from (3.4), or

$$c = \frac{\Gamma(\frac{1}{3})\Gamma(n/(n+1))}{3\Gamma((4n+1)/(3n+3))}. \quad (3.9)$$

Multiplying (3.8) by f and integrating, (3.5) leads to the following relation between U and h , namely

$$U(x)h(x) = \frac{c}{F_n}, \quad (3.10)$$

where $F_n = \Gamma(\frac{2}{3})\Gamma(n/(n+1))/3\Gamma((5n+2)/(3n+3))$. Equation (3.7) can now be integrated using (3.10) to obtain the expression for the streamwise velocity component at the free surface, or

$$U(x \geq x_0) = \begin{cases} \left[\frac{n+1}{3n(2n-1)F_n^{n+1}} \frac{1}{(x+l)} \right]^{1/(2n-1)}, & n \neq \frac{1}{2}, \\ e^{-1.3297x+l}, & n = \frac{1}{2}, \end{cases} \quad (3.11)$$

as well as the film thickness

$$h(x \geq x_0) = \begin{cases} c \left[\frac{3n(2n-1)}{(n+1)F_n^{n-2}} (x+l) \right]^{1/(2n-1)}, & n \neq \frac{1}{2}, \\ 1.461e^{1.3297x-l}, & n = \frac{1}{2}. \end{cases} \quad (3.12)$$

Here l is an integration constant, which is determined upon matching the solution with that from the developing boundary-layer region (ii) ($x < x_0$). Clearly, from (3.9), c is positive. In this case, (3.11) and (3.12) indicate, as expected, that U and h are decreasing and increasing functions of x , respectively, for any fluid. Finally, note that (3.11) and (3.12) reduce to Watson's results (1964) for planar Newtonian jet if $n = 1$. In this case, no further treatment is required. In contrast, for power-law fluids, additional issues require further consideration.

3.1. Asymptotic form of the outer-layer solution for $\eta \rightarrow 1$

The third boundary condition in (3.4) indicates that, as $\eta \rightarrow 1$, the leading-order term in the viscosity expression (2.3) vanishes for shear-thickening fluids, and becomes infinite for shear-thinning fluids. In this case, the thin-film approximation for a power-law fluid becomes invalid near the free surface. This anomaly is also encountered in the boundary-layer flow of power-law fluids, which was considered by Denier & Dabrowski (2004). Following their treatment, a thin outer adjustment viscous layer near the free surface is introduced in order to smooth out the inner solution as the free surface is approached. The inner and outer layers for the region $x > x_0$ are schematically illustrated in figure 2 for a shear-thinning fluid. The layers in the developing boundary layer region ($x < x_0$) are also shown in the figure for later reference.

In order to determine the correct flow structure near the free surface ($\eta \rightarrow 1$), a shift in origin is taken by setting $z = 1 - \eta$ (see figure 2). In this case, the small- z asymptotic

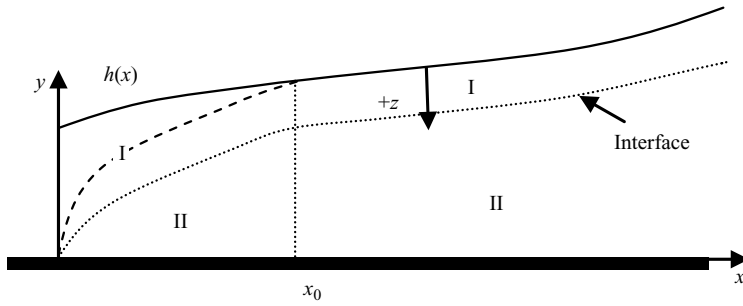


FIGURE 2. Outer- (I) and inner-layer (III) domains in the developing ($x < x_0$) and fully developed viscous ($x > x_0$) boundary-layer flow regions schematically illustrated for shear-thinning fluid. The boundary layer is shown as dashed curve.

form for f can be written as

$$f = 1 + \gamma z^b, \quad 0 < z \ll 1, \tag{3.13}$$

which, upon substitution in (3.7), gives $b = (n + 1)/n$. In this case, γ is negative and is given by

$$\gamma = -3^{1/n} \left(\frac{nc}{n + 1} \right)^{(n+1)/n}. \tag{3.14}$$

The asymptotic form (3.13) is valid in the outer-layer region, including the interface between the inner and outer layers. This form allows the imposition of boundary conditions at the interface (at some suitable small z) and therefore the integration of (3.7), thus leading to the inner solution of the problem. The thickness of the outer layer or the position of the interface is estimated next.

3.2. Estimation of the outer-layer thickness and the inner-layer solution

Evaluation of the higher-order terms in the viscosity expression (2.3) indicates that some of these terms become important as $\eta \rightarrow 1$, and therefore cannot be neglected. In particular, using the asymptotic form (3.13), the order of the two dominant terms in (2.3) for small z is found to be $u_y^2 \sim (U/h)^2 z^{2/n}$ and $\varepsilon^2 u_x^2 \sim Re^{-2} U^2$. The two terms become comparable when $z = O(Re^{-n})$. It is therefore at this height that the simple power-law expression $\mu = |u_y|^{n-1}$ for the viscosity of a thin film is expected to break down. This simultaneously gives an estimate of the thickness of the outer layer and the position of the interface. Clearly, the outer layer is expected to be small since Re is relatively large ($Re \gg 1$). The thickness of the outer layer is smaller for the more shear thickening fluids. Now that the interface position is estimated, f in turn is determined by integrating (3.7) over the inner-layer region, between the plate $z = 1$ and the interface. The integration is started at the interface using a fourth-order Runge–Kutta quadrature routine, coupled with a simple bisection scheme to determine the unknown c (and γ), until the boundary condition at the plate is satisfied to within some desired tolerance, of $O(10^{-6})$. Expression (3.9) provides an initial guess for c . The thickness of the outer layer or the position of the interface depends on Re , and, in turn, should affect the inner solution. However, calculations show that the choice of Re does not change significantly the velocity profile in the inner layer, but changes only the position of the interface. The influence of shear thinning and shear thickening on the flow is examined through the similarity profiles $f(\eta)$ shown in figure 3. The actual velocity profiles are shown in figure 16. Although the velocity profiles remain

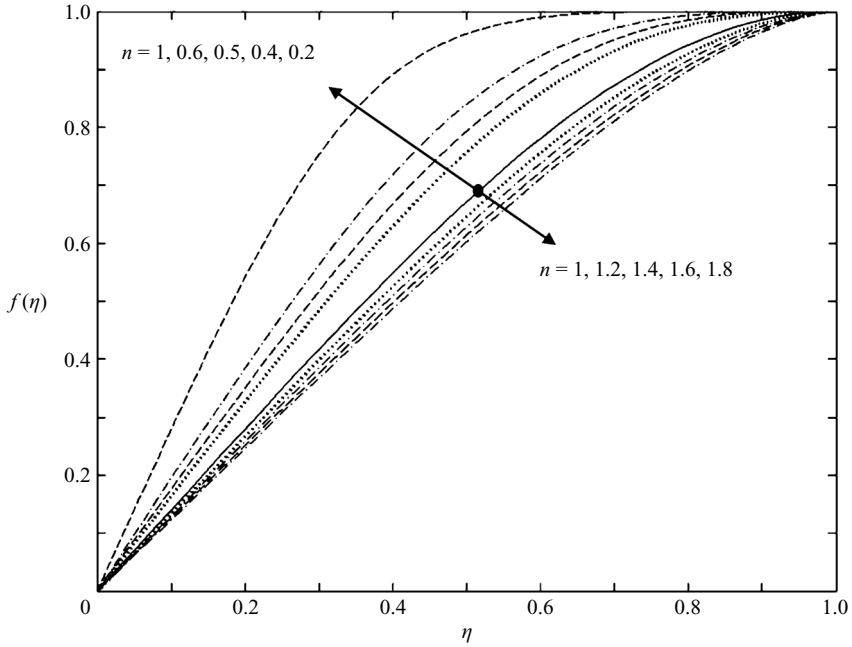


FIGURE 3. Velocity profiles $f(\eta)$ in the fully viscous boundary-layer region ($x > x_0$) for shear-thinning and shear-thickening jets.

qualitatively unchanged as n is varied, a couple of observations can be made. For shear-thinning fluids ($n < 1$), the power-law index n has a stronger influence on the slope of the profiles near the plate and free surface. As n decreases the inviscid limit behaviour (plug flow) is clearly approached. The slope of f at the plate, $f'(\eta = 0)$, is an important characteristic of the solution because of its relation to the shear stress at the plate, $\tau_0(x) \equiv \tau_{xy}(x, y = 0)$, which, in dimensionless form, is

$$\tau_0(x > x_0) = \mu u_y|_{y=0} = \frac{1}{Re} \left(\frac{U}{h} \right)^n [f'(0)]^n. \tag{3.15}$$

Here ρU_0^2 is taken as a reference for the shear stress and $\mu = u_y^{n-1}$. Figure 4 shows the dependence of $f'(\eta = 0)$ on n , indicating an apparent decrease in shearing for the more shear-thickening fluids. However, the exact value of the shear stress at the plate is of course established only when the film thickness h and velocity U are determined (see later). As mentioned earlier, the analytical expression for c in (3.9) is used as an initial guess to obtain the numerical solution. It is found that the analytical prediction $f'(\eta = 0) = c$ agrees to within 10^{-4} with its exact value shown in figure 4. This confirms the validity of the analytical expressions (3.11) and (3.12) for the film velocity and profile, respectively.

3.3. Outer-layer solution

The flow field in the outer layer in region (iii) is now determined by first letting $y = h(x) - Re^{-n}\xi$. In this case, $z = Re^{-n}(\xi/h)$, and $\xi = O(1)$. The asymptotic form (3.13), and expressions (3.3) and (3.6), suggest the following form for the velocity components in the outer layer region, namely

$$u = U(x) + Re^{-(n+1)}U_1(x, \xi) + \dots, \quad v = Uh' + Re^{-n}V_1(x, \xi) \dots, \tag{3.16}$$

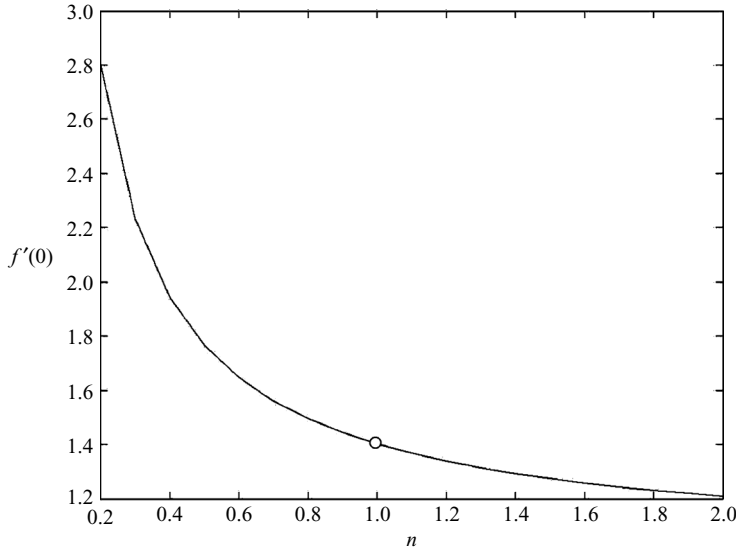


FIGURE 4. Dependence of the velocity gradient $f'(0)$ at the plate on the power-law index n in the fully viscous boundary-layer region ($x > x_0$). \circ , $n = 1$, $f'(0) = 1.40218$ (Watson 1964).

where higher-order terms are clearly negligible at large Reynolds number. At the interface, $U_1(x, \xi)$ and $V_1(x, \xi)$ are found to be

$$U_1(x, \xi) = U\gamma \left(\frac{\xi}{h}\right)^{(n+1)/n}, \quad V_1(x, \xi) = -\frac{h'U}{h}\xi \quad \text{as } \xi \rightarrow \infty. \quad (3.17)$$

On the other hand, substitution of u and v from (3.16) into the streamwise momentum equation (2.4*b*) leads, after some simplification, to the following equation for $U_1(x, \xi)$:

$$UU' = \frac{\partial}{\partial \xi} \left(\mu_1 \frac{\partial U_1}{\partial \xi} \right), \quad (3.18)$$

where the viscosity function μ_1 is given by

$$\mu_1 = \left[\left(\frac{\partial U_1}{\partial \xi} \right)^2 + 2U'^2 + 2 \left(\frac{h'U}{h} \right)^2 \right]^{(n-1)/2}. \quad (3.19)$$

Equation (3.18) must be integrated subject to the following boundary conditions:

$$U_1(\xi = 0) = 0, \quad U_1 \rightarrow U\gamma (\xi/h)^{(n+1)/n} \quad \text{as } \xi \rightarrow \infty. \quad (3.20)$$

These conditions ensure the correct asymptotic decay of U_1 near the free surface ($\xi \rightarrow 0$), and the correct form at the interface ($\xi \rightarrow \infty$). Equation (3.18) is conveniently rescaled by letting $U_1 = b_0F$, $\xi = b_1\zeta$ where $b_0 = B^{(n+1)/2}/(UU')$, $b_1 = -\alpha B^{n/2}/(UU')$, with $B = 2(U')^2 + 2(h'U/h)^2$. From (3.9), c is positive, and thus from (3.7), $U'(x)$ is negative. Therefore b_0 is negative and b_1 is positive since B is positive. In this case, the equation for $F(\zeta)$ can be obtained from (3.18) and (3.19)

$$\frac{d}{d\zeta} [(F')^2 + 1]^{(n-1)/2} F' = 1, \quad (3.21)$$

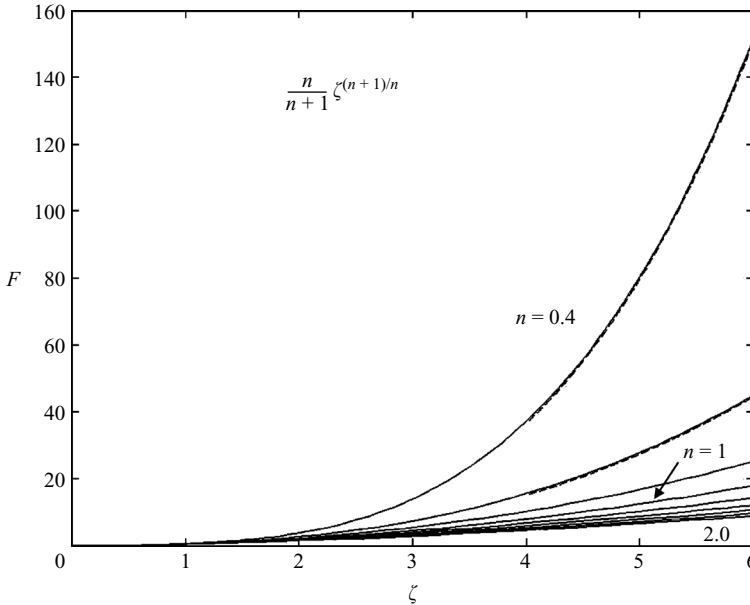


FIGURE 5. Plots of F versus ζ for $n=0.4, 0.6, 0.8, \dots, 2$. Asymptotic solutions (dashed curves) are also shown for shear-thinning jets.

which must be integrated subject to the following boundary conditions:

$$F(\zeta = 0) = 0, \quad F \rightarrow \frac{n}{n+1} \zeta^{(n+1)/n} \quad \text{as } \zeta \rightarrow \infty. \tag{3.22}$$

If (3.21) is integrated once with respect to ζ , the asymptotic condition $F' \rightarrow \zeta^{1/n}$ as $\zeta \rightarrow \infty$ can be simultaneously satisfied, leading to

$$((F')^2 + 1)^{(n-1)/2} F' = \zeta. \tag{3.23}$$

It is clear from (3.23) that $F'(0)=0$. This condition can then be used as a second (initial) boundary condition, in addition to $F(0)=0$, and (3.21) is integrated numerically subject to the two homogeneous initial conditions. The profiles $F(\zeta)$ for both shear-thinning ($n < 1$) and shear-thickening ($n > 1$) fluids are shown in figure 5. The special case for a Newtonian fluid ($n=1$) is also included, which corresponds to $F=\zeta^2/2$. Recalling the definition of F , it is observed from figure 5 that the drop in velocity from its value at the free surface increases strongly for the more shear-thinning fluids. In addition, the asymptotic form in (3.20) indicates that this drop is more significant for a flow with larger free-surface velocity. Finally, the asymptotic behaviour for F is added to the figure for reference, which also reflects the smoothness between the inner- and outer-layer solutions.

4. Developing boundary-layer flow ($x < x_0$)

In region (ii), or the developing boundary-layer region ($1/Re \ll x < x_0$), the flow is assumed to be sufficiently inertial for inviscid flow to prevail between the boundary-layer limit and the free surface (see figure 1). In this case, (2.4a) and (2.5) must be solved subject to conditions (2.6) and the following condition outside the

boundary layer:

$$u(1/Re < x < x_0, \quad \delta \leq y < h) = 1. \tag{4.1}$$

The developing boundary-layer equations can be solved numerically or approximately. Both approaches are considered in the present work. The approximate solution will be outlined in § 6. Since the free-stream velocity is constant (equal to 1), the boundary-layer equations admit a self-similar profile. The streamfunction is then expressed as

$$\psi = x^{1/(n+1)} \bar{f}(\bar{\eta}), \tag{4.2}$$

where the similarity variables \bar{f} and $\bar{\eta}$ are re-defined here. In this case,

$$u = \frac{\partial \psi}{\partial y} = \bar{f}'(\bar{\eta}), \quad v = -\frac{\partial \psi}{\partial x} = \frac{x^{-n/(n+1)}}{n+1}(\bar{\eta} \bar{f}' - \bar{f}), \tag{4.3}$$

where $\bar{\eta} = yx^{-1/(n+1)}$. In region (ii), the total depth h of the flow is $O(1)$ because of continuity. Similarly to Newtonian fluids, it is not difficult to show that the dimensional boundary-layer thickness for power-law fluids can be estimated by assessing the order of each term in the boundary-layer equations, leading to $\delta^* = O(mU_0^{n-2}x^*)^{1/(n+1)}$. Equivalently, the order of magnitude for the dimensionless boundary-layer thickness is $\delta = O(x^{1/(n+1)})$. Thus, the boundary-layer thickness becomes comparable with h when $x = O(1)$ or $x^* = O(aRe)$. Consequently, since the solution (4.2) is valid only when $x^* \gg a$, the Reynolds number of the incident jet must be large, or $Re \gg 1$. In region (iii), $x = O(1)$, and the speed at the free surface is of the same order of magnitude as U_0 , so that $U = O(1)$. Also, since there is a transition from the Blasius-type profile (4.2) to the similarity solution (3.3), it follows from (3.11) that $x + l = O(1)$. Thus $l = O(1)$, of the same order as the length scale for the streamwise development of the boundary layer in regions (ii) to (iii). In this case, since Re is large, $l^* \gg a$. Watson (1964) argued that, ultimately the way in which the flow originates (at the stagnation point) becomes unimportant, and the similarity solution of § 3 is valid, with an appropriate choice of the length l . However, the value of l depends on the development of the flow in the inner regions, but its order of magnitude is possible to estimate at this stage as above. Upon substituting u and v into (2.4b), the following equation for \bar{f} is obtained, namely

$$\bar{f}''' + \frac{\bar{f}(\bar{f}')^{2-n}}{n(n+1)} = 0, \tag{4.4}$$

subject to the boundary conditions

$$\bar{f} = \bar{f}' = 0 \quad \text{at} \quad \bar{\eta} = 0, \quad \bar{f}' \rightarrow 1 \quad \text{as} \quad \bar{\eta} \rightarrow \infty. \tag{4.5}$$

This is a nonlinear problem of the two-point boundary-value type, which is solved numerically. Following Denier & Dabrowski (2004), the asymptotic form for \bar{f}' in the limit $\bar{\eta} \rightarrow \infty$ is expressed approximately as

$$\bar{f}' = 1 + A\bar{\eta}^{(n+1)/(n-1)} + \dots \tag{4.6}$$

where $A = -(2n)^{1/(1-n)} |(n+1)/(n-1)|^{n/(1-n)}$. This asymptotic form (4.6) clearly shows that for shear-thinning fluids ($n < 1$), $\bar{f}' \rightarrow 1$ as $\bar{\eta} \rightarrow \infty$. Note that for a Newtonian fluid ($n = 1$), (4.6) breaks down owing to the singularity in this limit. This indicates that \bar{f}' has faster than algebraic asymptotic behaviour for Newtonian fluids, which is reflected in the exponential behaviour of the solution of the classical Blasius flow over a flat plate (see also below). On the other hand, for shear-thickening fluids ($n > 1$), \bar{f}' fails to approach unity in the limit $\bar{\eta} \rightarrow \infty$. Moreover, no other asymptotic form

can be deduced from (4.4) for $n > 1$. In fact, it is observed that for shear-thickening fluids, equation (4.4), when solved subject to conditions (4.5), leads to an overshoot in velocity ($u > 1$) for large $\bar{\eta}$. This suggests that the boundary layer for shear-thickening fluids must have a finite thickness. This point was recognized first by Acrivos *et al.* (1960), who found that the boundary-layer region for shear-thickening fluids cannot be infinite as for Newtonian or shear-thinning fluids. Denier & Dabrowski (2004) re-visited this issue and observed that the boundary condition $\bar{f}'(\eta \rightarrow \infty) = 1$ does not describe the correct behaviour for shear-thickening fluids in the far-field region. They also pointed out that some care must be taken to ensure that the numerical solution satisfies the correct asymptotic behaviour.

Consequently, and following Denier & Dabrowski (2004), the problem for shear-thickening fluids is re-posed as a free-boundary problem, and the outer limit, $\bar{\eta} = \bar{\eta}_C$, of the boundary layer now becomes an unknown part of the problem. In this case, (4.4) is solved subject to the following boundary conditions

$$\bar{f}(\bar{\eta} = 0) = \bar{f}'(\bar{\eta} = 0) = 0, \quad \bar{f}'(\bar{\eta} = \bar{\eta}_C) = 1, \quad \bar{f}''(\bar{\eta} = \bar{\eta}_C) = 0. \quad (4.7)$$

The fourth condition in (4.7) ensures that the streamwise velocity component does not overshoot its far-field unity value at the outer edge of the boundary layer. This system may appear to be over-specified. However, $\bar{\eta}_C$ is regarded as unknown, and is thus determined by solving the two-point boundary-value problem (4.4) subject to conditions (4.7). Here, problem (4.4) may be compared to a free-surface flow problem, with $\bar{\eta}_C$ corresponding to the free-surface height, and the fourth condition in (4.7) corresponding to the kinematic condition. As suggested by Denier & Dabrowski (2004), it is useful to make a shift of coordinates so as to define the origin to be at the critical point $\bar{\eta} = \bar{\eta}_C$ (see figure 2). Thus, let $z = \bar{\eta}_C - \bar{\eta}$ represent the coordinate shift. In order to integrate numerically the transformed equation, the small- z asymptotic form for \bar{f} is employed to start the calculation at some suitably chosen Δz . This asymptotic form is readily shown to be

$$\bar{f} = \beta - z + \theta z^k, \quad (4.8)$$

which, upon substitution into (4.4), gives

$$\frac{1}{\theta} |\theta|^{2-n} = n(n+1)k^{n-1}(k-1)^{n-1}(k-2)\beta^{-1}, \quad k = \frac{2n-1}{n-1}. \quad (4.9)$$

Here β is an unknown, which is determined numerically. The asymptotic form (4.8) constitutes the boundary condition at the interface for the solution in the inner region, which is obtained by integrating (4.4) subject to the boundary conditions at the plate. The position of the interface is estimated next.

4.1. The inner-layer solution

Equation (4.4) is based on the assumption that its solution matches smoothly onto the outer inviscid flow. However, as Denier & Dabrowski (2004) pointed out, there exists a discontinuity in the far-field flow domain. This discontinuity is due to the power-law model for viscosity $\mu = |u_y|^{n-1}$, which becomes invalid in the far field. The power-law model is the simplified form of the viscosity function (2.3a) after neglecting higher-order terms in ε , and is only valid in regions with certain minimum shear rate. In the far field, where the velocity gradient tends to zero, the power-law model breaks down and becomes obviously unrealistic, leading to infinite viscosity for shear-thinning fluids ($n < 1$) and zero viscosity for shear-thickening fluids ($n > 1$). This anomaly is also the underlying cause of the need for a finite width of the

boundary layer for shear-thickening fluids. Denier & Dabrowski (2004) demonstrated, for both shear-thinning and shear-thickening fluids, that the simplified boundary-layer equations are only a first step in describing the flow behaviour for a power-law fluid at high Reynolds number. The discontinuity in flow can be smoothed out by introducing a thin viscous transition layer, which allows uniform matching with the outer inviscid flow. The flow domain where the power-law model is valid constitutes the inner layer. The inner and transition layers are schematically illustrated in figure 2 for $x < x_0$. Note that for shear-thickening fluids, the transition layer includes the $\bar{\eta}_c$ boundary.

For shear-thickening fluids, the inner solution can be obtained by integrating the transformed equation (4.4) with respect to z from the interface to the plate. The asymptotic form (4.8) constitutes the boundary condition at the interface. In order to determine the position of the interface, it is helpful to first observe that the evaluation of the higher-order terms in the viscosity expression (2.3) indicates that some of these terms become important as $\eta \rightarrow \bar{\eta}_c$, and therefore cannot be neglected. In particular, using the asymptotic form (4.8), the order of the two dominant terms in (2.3) for small z is found to be $u_y^2 \sim x^{-2/(n+1)}z^{2/(n-1)}$ and $\varepsilon^2 u_y v_x = Re^{-2}x^{-2}z^{1/(n-1)}$. The two terms become comparable when $z = O(Re^{-2(n-1)})$. It is therefore at this height that the simple expression $\mu = |u_y|^{n-1}$ is expected to break down. This simultaneously gives an estimate of the position of the interface. Clearly, this distance between the interface and the critical point η_c is expected to be small since Re is relatively large ($Re \gg 1$). Similarly to the fully viscous boundary-layer region (ii) in §3, the position of the interface is found to be higher for the more shear-thickening fluids. Now, since the interface position is estimated, \bar{f} in turn can be determined by integrating (4.4) from the interface, $z = O(Re^{-2(n-1)})$, to the plate ($z = \bar{\eta}_c$), where $\bar{f} = d\bar{f}/dz = 0$ is satisfied to within some desired tolerance, $O(10^{-6})$ in the present case. This was accomplished using a fourth-order Runge–Kutta quadrature routine, coupled with a simple bisection scheme to determine the unknown β (or equivalently θ) and $\bar{\eta}_c$.

Similarly, for shear-thinning fluids ($n < 1$), it is found that when $y = O(Re^{1-n})$, the viscosity expression (2.3) breaks down. This simultaneously gives an estimate of the position of the interface between the inner and transition layer. Clearly, the interface is far from the plate, i.e. $y = O(Re^{1-n}) \gg 1$, since Re is relatively large and $n < 1$. Therefore, the inner-layer solution for shear-thinning fluids can be easily obtained by integrating (4.4) using the first two boundary conditions of (4.5) at the plate and far-field asymptotic condition (4.6) where $\bar{\eta} = O(Re^{1-n})$. This was accomplished using a fourth-order Runge–Kutta quadrature routine, coupled with a simple bisection scheme to determine the unknown velocity gradient $\bar{f}''(0)$ at the plate.

The similarity profiles in the inner-layer region and for $x < x_0$ are shown in figure 6. The actual velocity profiles are shown in figure 16. It is observed from figure 6 that the similarity profile changes dramatically as the power-law index n is varied. While the dependence of \bar{f}' on n is monotonic (essentially linear) for shear-thickening fluids, approaching a plug-flow behaviour for large n , it is non-monotonic for shear-thinning fluids. The rate of approach towards the inviscid limit is much slower for the more shear-thinning fluid. This rate can be estimated from (4.6), which, for instance, is $O(\eta^{-1.5})$ for $n = 0.2$ and $O(\eta^{-4})$ for $n = 0.6$. Figure 7 shows the variation of the critical position $\bar{\eta}_c$ with n . The rate of decay of the critical position with n can be estimated for a fluid near Newtonian, and for large n to be, respectively,

$$\bar{\eta}_c \approx 0.018n^{-11.6} \quad (1 < n < 1.4), \tag{4.10a}$$

$$\text{and } \bar{\eta}_c \approx 8.2n^{-0.96} \quad (n > 2). \tag{4.10b}$$

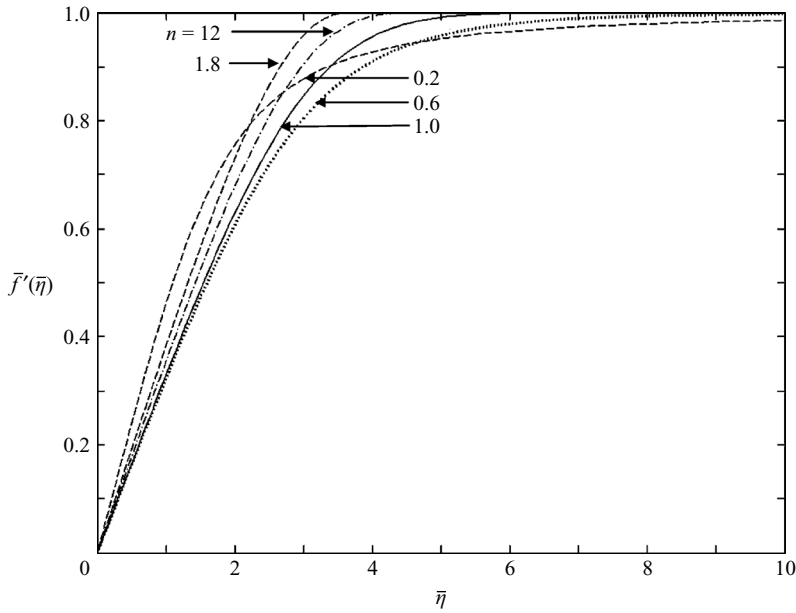


FIGURE 6. Velocity profiles $\bar{f}'(\bar{\eta})$ in the developing boundary layer region ($x < x_0$) for shear-thinning and shear-thickening jets.

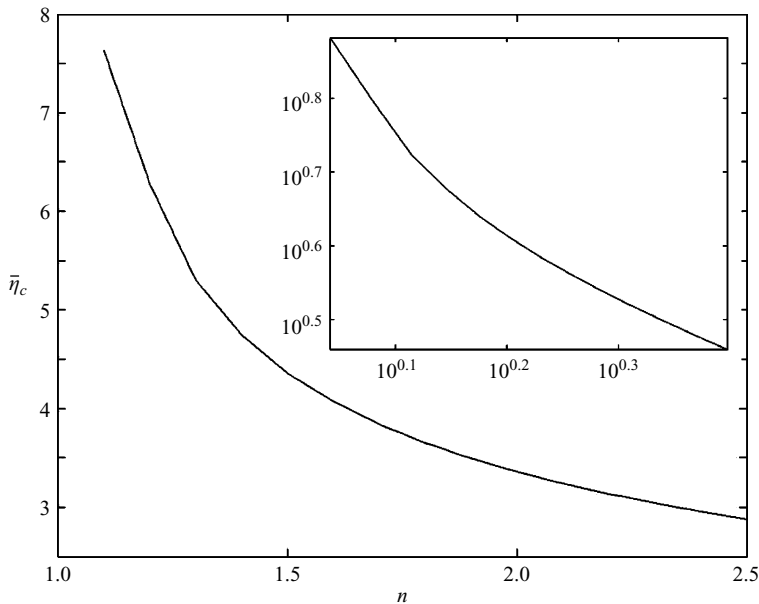


FIGURE 7. Dependence of the critical position $\bar{\eta}_c$ on n for shear-thickening fluids in the developing boundary layer region ($x < x_0$). Inset shows log–log plot.

The dimensionless shear stress at the plate defined in (3.15) now becomes

$$\tau_0(x < x_0) = \frac{[\bar{f}'(0)]^n}{Re x^{n/(n+1)}}, \tag{4.11}$$

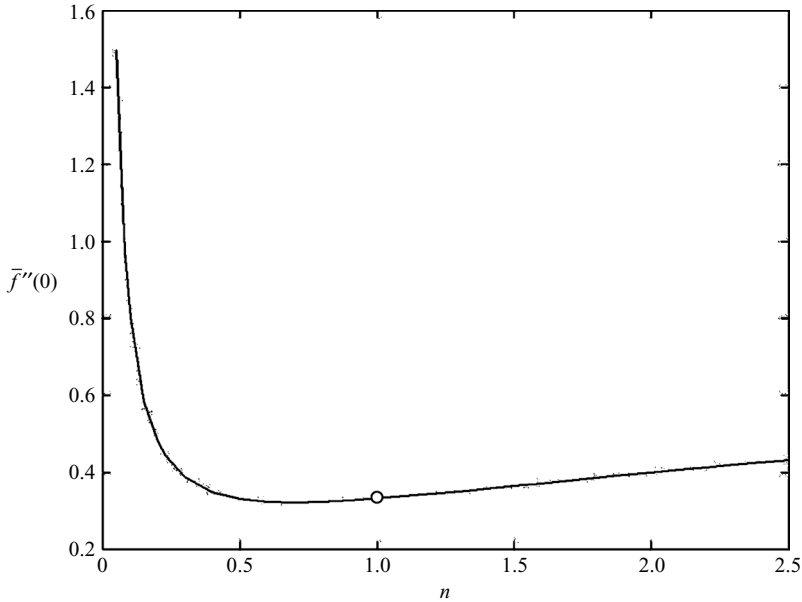


FIGURE 8. Dependence of the velocity gradient $\bar{f}''(0)$ at the plate on n in the developing boundary-layer region ($x < x_0$) \circ , $n = 1$ $\bar{f}''(0) = 0.33205$ (schlichting 1979).

which indicates that the shear stress at the plate decreases faster with x for shear-thickening fluids than for shear-thinning fluids, roughly as $1/x$ (for large n) and $1/x^n$ (for small n), respectively. The shear stress is established only when the extent of the developing boundary-layer region, x_0 , is determined (see later). For now, the extent of shearing in the developing boundary-layer region can be estimated from the value of $\bar{f}''(0)$. Figure 6 shows that the power-law index n has a strong influence on $\bar{f}''(0)$ for shear-thinning fluids. This complex dependence is depicted in figure 8, which displays a strong decay in shearing as n increases from zero. However, there is a minimum that follows at $n \simeq 0.7$, which suggests that this resistance to movement is halted as n increases. For weakly shear-thinning fluids ($n > 0.7$) and shear-thickening fluids, the fluid experiences increasing resistance to movement with n . In this case, the velocity gradient $f''(0) \approx 0.067n + 0.265$ (for $n > 1$). Figures 6, 7 and 8 therefore clearly illustrates the behaviour expected for highly shear-thinning ($n < 0.5$) and highly shear-thickening fluids ($n > 1.5$). In the former case, the jet tends to behave as a dilute gas upon impingement, exhibiting high shearing near the plate, but increasingly lesser movement as n decreases (see figure 6). In the latter case, the jet exhibits an increase in shearing near the plate as n increases, but only over a distance ($\bar{\eta}_c$) that is increasingly smaller (see again figures 6 and 7), with the fluid behaving close to Newtonian at greater distance. Of course, the jet behaves more like an ordinary fluid in the vicinity of the minimum in figure 8.

4.2. The viscous transition layer

In order to match the above inner-layer solution of (4.4) with the far-field flow ($u \rightarrow 1$ as $\bar{\eta} \rightarrow \infty$), an outer viscous transition layer is introduced. By including higher-order terms in the viscosity function, the correct momentum equation that describes the flow in the viscous transition layer is derived. This new momentum equation is solved by matching the transition-layer flow with the inner flow at the interface and with

the outer potential flow. Thus, the discontinuity in the flow domain is smoothed out and the inner solution is correctly matched with the outer potential flow. However, if the boundary-layer thickness is defined as the distance for which $\bar{f}' = 0.99$, for large impinging jet Reynolds number, the thickness of the inner layer is larger than the boundary-layer thickness. In fact, as was shown earlier, the thickness of the shear-thickening transition layer is $z = O(Re^{-2(n-1)})$ which is very small for large Re , and the shear-thinning transition layer is located at $y = O(Re^{1-n}) \gg 1$, which is far away from the plate. Therefore, the importance of the inner-layer region far exceeds that of the transition-layer region, and the latter can therefore be neglected. However, the matching procedure for shear-thickening fluids is still given for completeness.

For a shear-thickening fluid, the flow field in the transition layer is now determined by first letting $y = y_c - Re^{-2(n-1)}\bar{\xi}$. In this case, $z = Re^{-2(n-1)}x^{-1/(n+1)}\bar{\xi}$, and $\bar{\xi} = O(1)$. The asymptotic form (4.6) and expressions (4.3) suggest the following form of the velocity components in the outer-layer region, namely

$$u = 1 + Re^{-2n}\bar{U}_1(x, \bar{\xi}) + \dots, \quad v = \bar{V}_1(x) + \dots, \tag{4.12}$$

where the higher-order terms do not enter into the subsequent analysis for large Re . At the interface, the coefficients $\bar{U}_1(x, \bar{\xi})$ and $\bar{V}_1(x)$ are found to be

$$\bar{U}_1(x, \bar{\xi}) = -\theta kx^{-n/(n^2-1)}\bar{\xi}^{n/(n-1)}, \quad \bar{V}_1(x) = \bar{A}x^{-n/(n+1)} \quad \text{as } \bar{\xi} \rightarrow \infty, \tag{4.13}$$

where $\bar{A} = (\bar{\eta}_c - \beta)/(n + 1)$. In this case, the substitution of u and v from (4.12) into the streamwise momentum equation (2.4b) leads to

$$-\bar{V}_1 \frac{\partial \bar{U}_1}{\partial \bar{\xi}} = \frac{\partial}{\partial \bar{\xi}} \left(\bar{\mu}_1 \frac{\partial \bar{U}_1}{\partial \bar{\xi}} \right), \tag{4.14}$$

where the viscosity function $\bar{\mu}$ is given by

$$\bar{\mu}_1 = \left| \left(\frac{\partial \bar{U}_1}{\partial \bar{\xi}} \right)^2 - 2 \frac{\partial \bar{U}_1}{\partial \bar{\xi}} \frac{d\bar{V}_1}{dx} + \left(\frac{d\bar{V}_1}{dx} \right)^2 \right|^{(n-1)/2}. \tag{4.15}$$

The boundary conditions appropriate to (4.14) are

$$\bar{U}_1 \rightarrow 0 \quad \text{as } \bar{\xi} \rightarrow -\infty, \quad \bar{U}_1 = -\theta kx^{-n/(n^2-1)}\bar{\xi}^{n/(n-1)} \quad \text{as } \bar{\xi} \rightarrow \infty. \tag{4.16}$$

The correct asymptotic decay of the streamwise deviation velocity \bar{U}_1 in the far field ($\bar{\xi} \rightarrow -\infty$) and the matching to the algebraic term in the inner layer ($\bar{\xi} \rightarrow \infty$) are ensured through these conditions. It is convenient to rescale (4.14) by defining $\bar{U}_1 = \bar{b}_0 \bar{f}$, $\bar{\xi} = \bar{b}_1 \bar{\zeta}$, where $\bar{b}_0 = (1/\bar{V}_1)(-d\bar{V}_1/dx)^n$ and $\bar{b}_1 = (1/\bar{V}_1)(-d\bar{V}_1/dx)^{n-1}$. Note $d\bar{V}_1/dx$ is negative from (4.13) and \bar{b}_0, \bar{b}_1 positive. In this case the equation for $\bar{F}(\bar{\zeta})$ becomes

$$\bar{F}' = \frac{d}{d\bar{\zeta}} (|\bar{F}' - 1|^{n-1} \bar{F}'), \tag{4.17}$$

subject to the following boundary conditions:

$$\bar{F} \rightarrow 0 \quad \text{as } \bar{\zeta} \rightarrow -\infty, \quad \bar{F} = - \left(\frac{n+1}{\bar{\eta}_c - \beta} \right)^{1/(n-1)} \theta k \bar{\zeta}^{n/(n-1)} \quad \text{as } \bar{\zeta} \rightarrow \infty. \tag{4.18}$$

Note the prime in (4.17) denotes the total differentiation with respect to $\bar{\zeta}$. Following Denier & Dabrowski (2004), a phase diagram in the (\bar{F}', \bar{F}'') plane is given in figure 9. It is found that a smooth solution exists only when $\bar{F}' < 0$, for which \bar{F}'' is strictly negative. Plots of \bar{F} versus $\bar{\zeta}$ are given in figure 10, from which it is shown that the

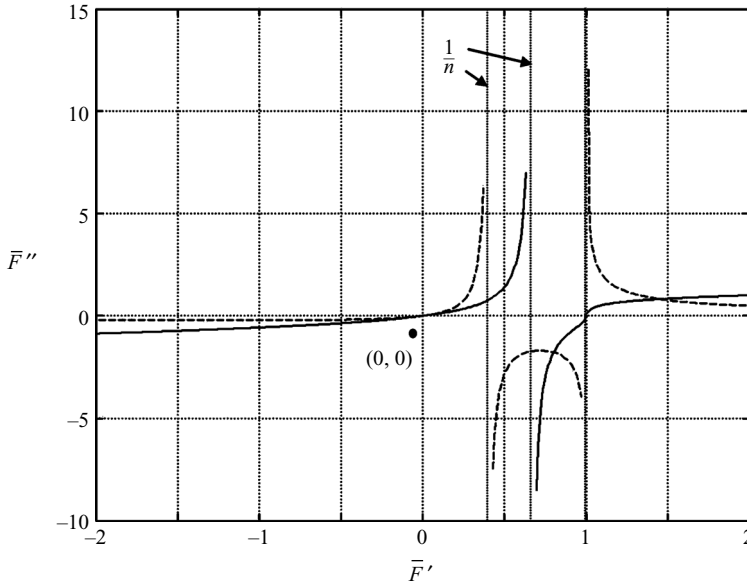


FIGURE 9. Typical phase plots in the (\bar{F}', \bar{F}'') plane for shear-thickening fluids for $n = 1.8$ (solid curves) and $n = 2.2$ (dashed curves).

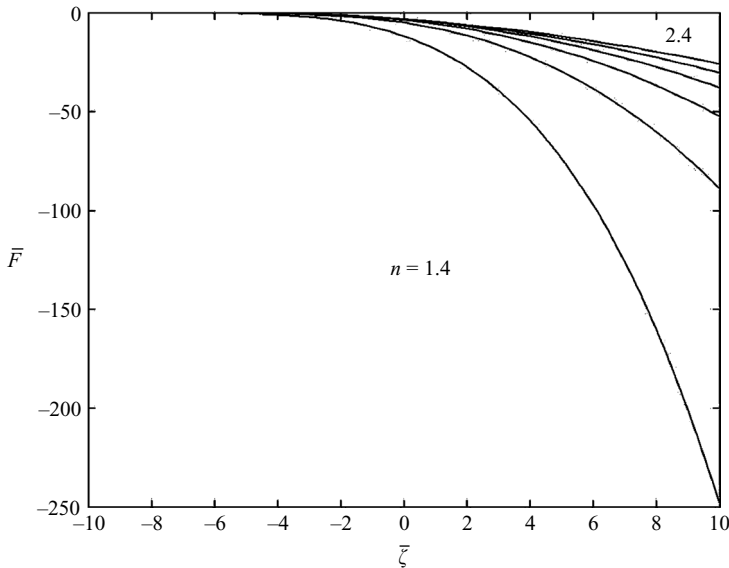


FIGURE 10. Plots of \bar{F} versus $\bar{\zeta}$ for $n = 1.4, 1, \dots, 2.4$.

discontinuity of the solution that arises near the critical position can be smoothed out within the viscous transition layer.

5. Matching process and composite flow

The flow in the entire physical domain is now obtained upon matching at $x = x_0$ the flows between the developing and fully viscous boundary-layer regions. Given

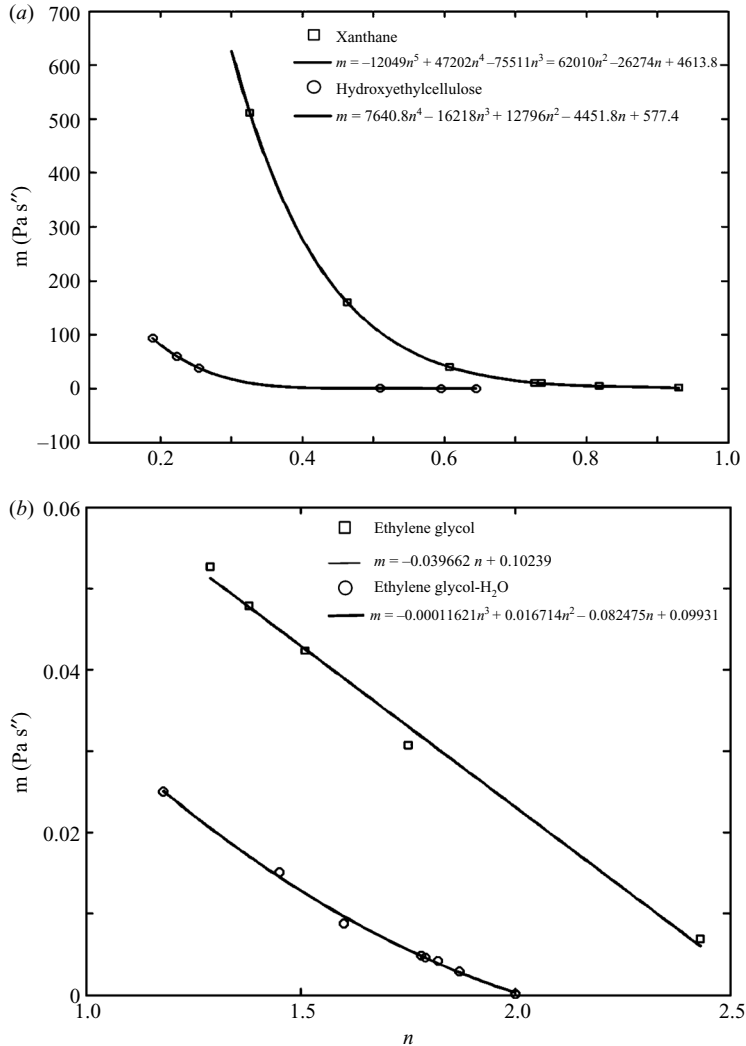


FIGURE 11. Experimental data showing the dependence of m on n and fitting curves: (a) Shear-thinning solutions: xanthane and hydroxyethylcellulose; (b) Shear-thickening solutions: ethylene glycol and ethylene glycol in water.

the complex scaling used in the formulation, some of the predictions are more effectively interpreted using real fluids. Consider then two shear-thinning fluids: xanthane (Lindner, Bonn & Meunier 2000) and hydroxyethylcellulose (Bird *et al.* 2002) solutions, and two shear-thickening fluids (Green & Griskey 1968): ethylene in glycol and ethylene in glycol/water solutions, with different levels of concentration, including the Newtonian limit. Figure 11 shows the dependence of m on n for each fluid based on experimental data. For shear-thinning fluids (figure 11a), m tends to decrease rather sharply with n , whereas for shear-thickening fluids (figure 11b), m tends to decrease linearly with n . Simple fit of the data allows the unambiguous interpretation of the results below in terms of n only. In this work, only xanthane and ethylene in glycol solutions will be used subsequently. The viscosity dependence on shear rate for these two solutions is given in figure 12 for each fluid, for different

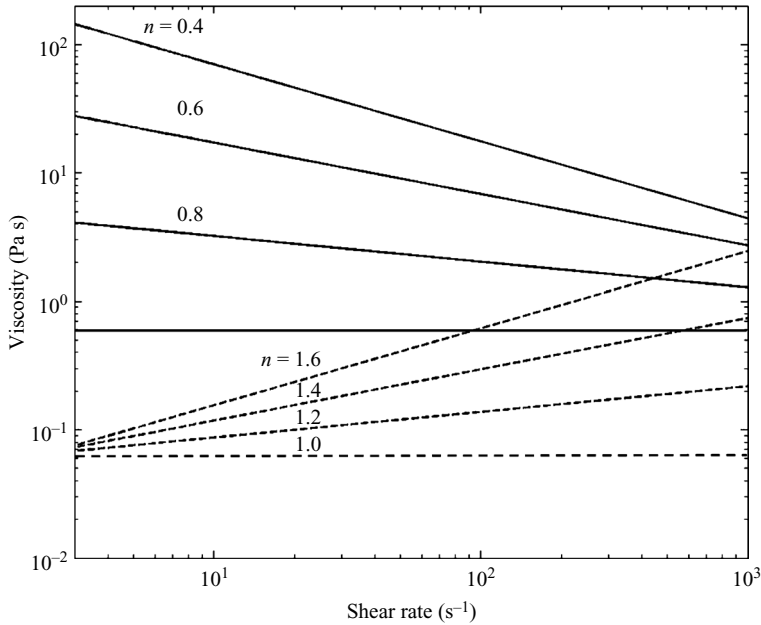


FIGURE 12. Viscosity dependence on shear rate for xanthane (solid curves) and ethylene glycol (dashed curves) solutions for various values of n .

n values. It is important to note from the figure that the ethylene in glycol solution is simultaneously more viscous and more shear thickening. In contrast, the overall viscosity of xanthane is higher when it is more shear thinning. This interplay between the overall level of viscosity and degree of shear thinning will have an intricate influence on the flow and jet profile.

Before discussing the matching at $x = x_0$, it is useful to summarize the flow structure in the developing and fully developed boundary-layer regions. In contrast to non-Newtonian fluids, the flow field for Newtonian fluids in regions (ii) and (iii) is governed by a similarity solution that is uniformly valid over the entire thickness of the film. For non-Newtonian fluids, anomalous behaviour arises at the approach of the inviscid flow or free surface. In region (ii), the viscosity becomes infinite for $n < 1$, and the velocity overshoots its inviscid value for $n > 1$. This difficulty is overcome by including the elongation terms in the viscosity expression that are otherwise negligible in boundary-layer or thin-film theory, therefore necessitating more than one layer above the plate. For $n < 1$, the flow domain comprises the inner layer, which is dominated by shearing, and the outer layer, which starts at a height $y = O(Re^{1-n})$ and extends over the entire inviscid region. For $n > 1$, the flow domain is allowed to extend only over a finite height $y_c(x) = \bar{\eta}_c x^{1/(n+1)}$, which grows with x but remains $O(1)$, since $\bar{\eta}_c = O(1)$ itself. The boundary-layer thickness $\delta(x) = \bar{\eta}_\delta x^{1/(n+1)}$ where $\bar{\eta}_\delta$ depends on n and satisfies $\bar{f}'(\bar{\eta} = \bar{\eta}_\delta) = 0.99$. Thus, $\bar{\eta}_\delta = O(1)$, so that $y_c \approx \delta = O(1)$. Immediately below y_c lies a transition layer to the inner region of thickness $O(Re^{-2(n-1)})$. In the fully viscous region (iii), the viscosity becomes infinite for $n < 1$ and zero for $n > 1$ at the approach of the free surface, therefore there is a need for a transition layer of thickness $O(Re^{-n})$ between the free surface and the inner region.

Consider now the matching of the developing and the fully developed boundary-layer flows at $x = x_0$. For shear-thinning fluids, the outer layer is much farther above the boundary-layer limit, so that the boundary-layer height in region (ii) can be

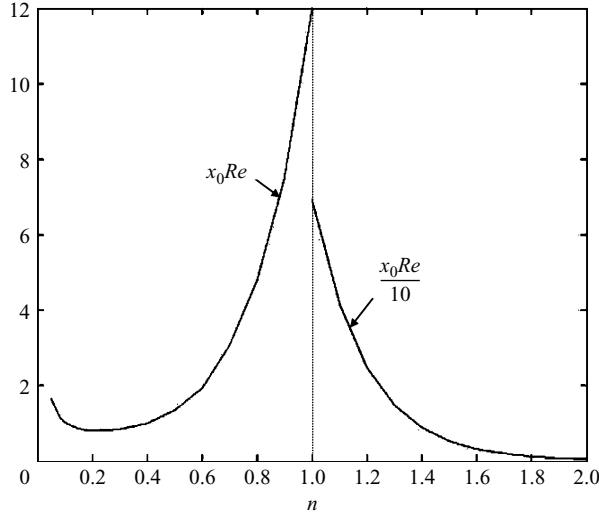


FIGURE 13. Dependence of the position of transition point, $x_0 Re$, on n for shear-thinning and shear-thickening jets.

matched either onto the interface height or onto the free surface in region (iii) at x_0 . Both alternatives will lead essentially to the same result given the small thickness of the transition layer below the free surface. Similarly for shear-thickening fluids, the transition layer in regions (ii) is sufficiently thin to be ‘confounded’ with the boundary-layer height. The transition layer in region (iii) is even thinner with thickness ratio $O(Re^{-2(n-1)}/Re^{-n} = Re^{2-n})$; recall that $n < 2$ (see Acrivos *et al.* 1960). In sum, it is emphasized that the primary purpose behind introducing the multi-layered structure in the developing and fully developed boundary-layer regions (ii) and (iii) is to smooth out the flow variables throughout the flow depth in each region. Given the small thickness of the transition layers, the matching between the two regions at $x = x_0$ is carried out only by matching the boundary-layer height to the film free surface. This is the only condition required to determine the flow field throughout the film domain.

Since $U(x_0) = 1$ and $\delta(x_0) = h(x_0)$, the matching position or length of the developing boundary-layer region, x_0 , is obtained from (3.10):

$$x_0 = \frac{c^{n+1}}{\bar{\eta}_\delta^{n+1} F_n^{n+1}}. \tag{5.1}$$

Figure 13 shows the dependence of x_0 on n , for both shear-thinning and shear-thickening fluids. x_0 exhibits a minimum for shear-thinning fluids at $n \approx 0.23$. For shear-thickening fluids, x_0 tends to decrease monotonically and rather sharply near the Newtonian limit. Consequently, both weakly shear-thinning ($n > 0.5$) and weakly shear-thickening ($n < 1.5$) jets appear to spread more easily. However, this apparent inconsistency between the two is resolved once the overall viscosity is considered (see figure 12). The non-monotonic response of the shear-thinning fluid is also a result of the intricate interplay between the overall viscosity level and the degree of shear-thinning. However, some caution is in order here when interpreting the results for the very shear-thinning fluid. Indeed, for $n < 0.4$, figure 13 indicates that $x_0 \sim 1/Re$ or, in dimensional terms, $x_0^* \sim a$. This means that the transition point is located too close to the stagnation or impingement point, which violates the basic assumption for the

validity of the current boundary-layer formulation. In addition, this corresponds to relatively small values of n , which in turn corresponds to a range of unrealistic fluids or fluids with too high a viscosity (see figure 12). More insight into the non-Newtonian effects is gained once the film profile is obtained (see the following).

The composite film thickness, $h(x)$, and free-surface velocity, $U(x)$, are obtained by considering first the conservation of mass equation in the developing boundary-layer region:

$$x^{1/(n+1)} \int_0^{\bar{\eta}_\delta} \bar{f}' d\bar{\eta} + h(x) - \delta(x) = 1 \quad (x \leq x_0). \tag{5.2}$$

The integral is evaluated by setting $x = x_0$ in (5.2) and using (5.1). In this case, the film thickness in the developing boundary-layer region is determined, or

$$h(x \leq x_0) = 1 + \bar{\eta}_\delta \left[1 - \frac{F_n}{c} \right] x^{1/(n+1)}. \tag{5.3}$$

The integration constant l that appears in (3.11) and (3.12) is now determined by first recalling that $U(x = x_0) = 1$, and evaluating (3.11) at $x = x_0$, leading to

$$l = \begin{cases} \frac{(n+1)\bar{\eta}_\delta^{n+1} - 3n(2n-1)c^{n+1}}{3n(2n-1)\bar{\eta}_\delta^{n+1}F_n^{n+1}}, & n \neq \frac{1}{2}, \\ 2.3482(\bar{\eta}_\delta)^{-3/2}, & n = \frac{1}{2}. \end{cases} \tag{5.4}$$

Hence, the film thickness $h(x)$ is given by (5.3) for $x < x_0$ and (3.12) for $x \geq x_0$, while the free surface velocity becomes $U(x < x_0) = 1$, and is given by (3.11) for $x \geq x_0$. It is observed that l is found numerically to be positive for $n > 1/2$. Expression (5.4) clearly shows that l is negative for $n < 1/2$. Figures 14 and 15 show the variation of the film thickness $h(x)$, boundary-layer thickness, $\delta(x)$, and shear stress at the plate, $\tau_0(x)$, with distance from impingement, for shear thinning and shear-thickening fluids, respectively. Here, the more suitable position variable, $xRe = x^*/a$ is used. The location, x_0Re , of the transition between the developing and fully developed flows is also indicated. Again, the fluids chosen are those reported in figure 12. Generally, $h(x)$ and $\tau_0(x)$ increases and decreases, respectively, with x owing to resistance from the plate, at a rate that is stronger for the more viscous fluid. The growth of the boundary-layer thickness is commensurate with that of the free surface, but $\delta(x)$ grows at a higher rate than $h(x)$. The shear stress decreases monotonically with x . For shear-thinning fluids, figure 14(a) shows enhanced thickening of the film in the fully viscous region ($x > x_0$), especially for the more viscous and strongly shear-thinning fluids ($n = 0.4$; see also figure 12), accompanied by a relatively milder drop in shear stress (figure 14b). However, there is a sharp drop in shear stress further downstream for $n = 0.4$, pointing to the strong difficulty of the fluid in spreading, leading essentially to a plug-flow scenario. Recall that, in the developing boundary-layer region ($x < x_0$), the free-surface velocity is always equal to one-keeping the stress level higher than for $x > x_0$, where the surface velocity decreases with x . Note the similarity between the pronounced increase in film thickness in region (iii) shown in figure 14(a) and the steep boundary-layer in the stagnation-flow region (i) depicted schematically in figure 1. The profiles for shear-thickening fluids are depicted in figure 15. In this case, figure 15(a) shows the gradual increase in film height and boundary-layer thickness with viscosity and level of shear thickening. More importantly, figure 15(b) shows the very rapid decrease in shear stress at large distance for the more viscous fluids ($n = 1.6$). Observe the difference in qualitative response for strongly shear-thinning

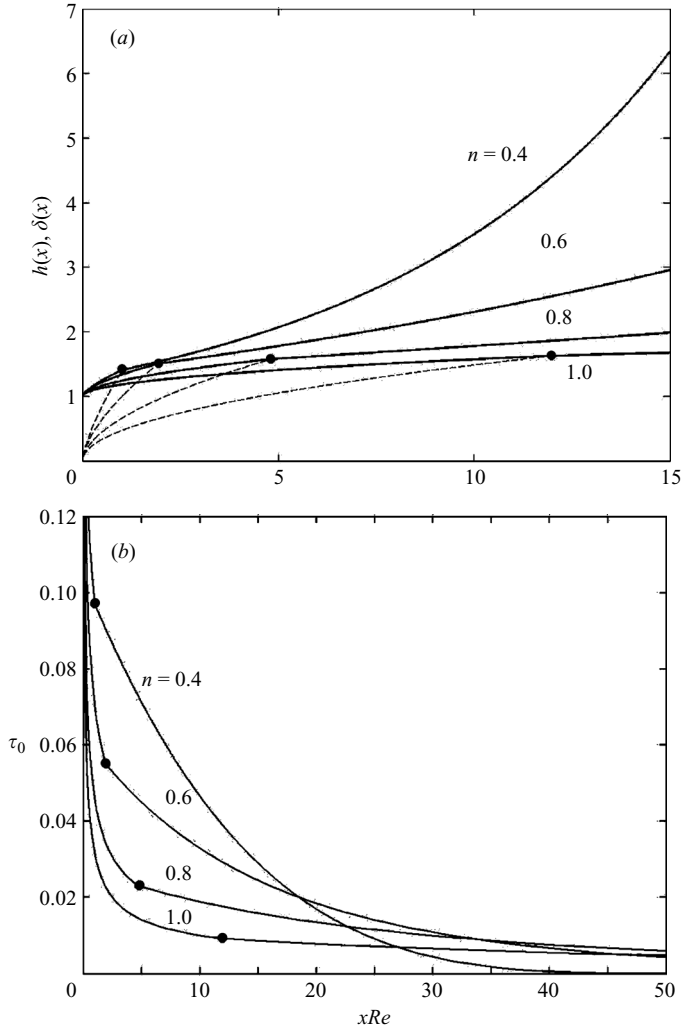


FIGURE 14. Influence of shear-thinning effect on: (a) the film thickness, $h(x)$, and the boundary-layer thickness, $\delta(x)$; (b) the shear stress at the plate, $\tau_0(x)$. Here, $U_0 = 8 \text{ m s}^{-1}$, $a = 0.008 \text{ m}$ and $\rho = 998 \text{ kg m}^{-3}$. Solid circles show location of transition point.

fluids compared to the weakly shear-thinning fluids. Consider again the fluid with $n=0.4$ from figure 14. The flow exhibits a change in concavity for $h(x)$ and a change in slope for $\tau_0(x)$ at the transition point. The emergence of a discontinuity does not occur for moderately shear-thinning fluids or shear-thickening fluids. In sum, highly viscous fluids that are strongly shear thinning (see figure 12 for $n=0.4$) spread with difficulty, even compared to highly viscous and simultaneously highly shear-thickening fluids. This illustrates the intricate flow behaviour resulting from the interplay between the shear-thinning character and the overall viscosity of the fluid.

Finally, the flow nature is further explored by showing the velocity profiles. Although the similarity profiles in figures 3 and 6 should allow the inference of the flow field, they do not lend themselves to immediate physical interpretation. Figure 16 displays the streamwise velocity distribution at difference locations. The profiles are shown over the same distance for typical shear-thinning ($n=0.6$) and shear-thickening ($n=1.4$) fluids

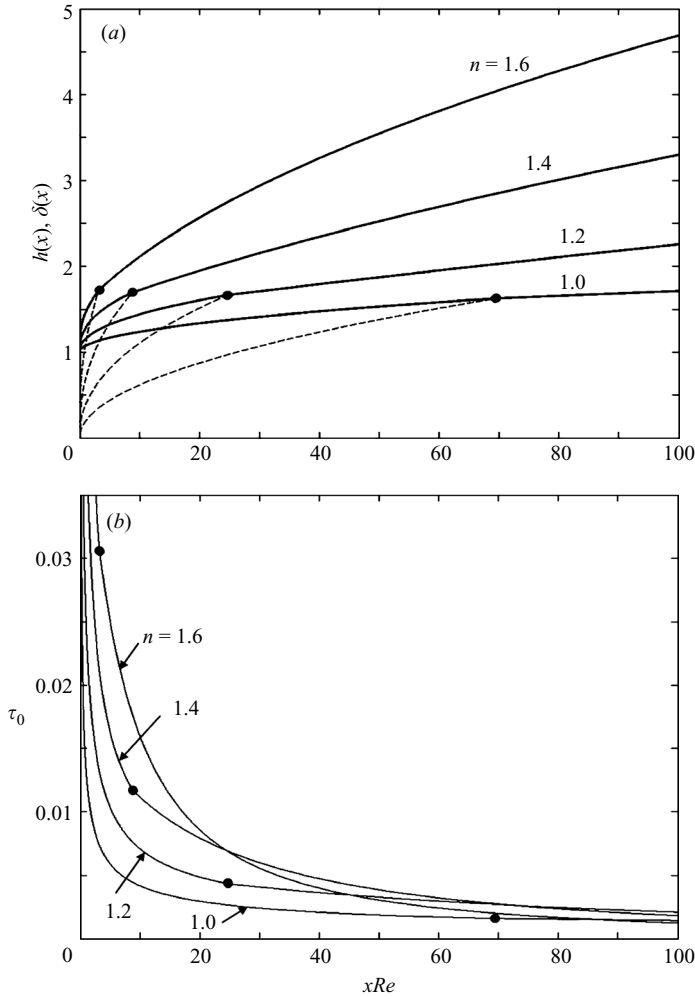


FIGURE 15. Influence of shear-thickening effect on: (a) the film thickness, $h(x)$, and the boundary-layer thickness, $\delta(x)$; (b) the shear stress at the plate, $\tau_0(x)$. Here, $U_0 = 5 \text{ m s}^{-1}$, $a = 0.008 \text{ m}$ and $\rho = 998 \text{ kg m}^{-3}$. Solid circles show location of transition point.

in figures 16(a) and 16(b), respectively. Clearly, the difficulty of the shear-thinning fluid in spreading is correlated with a smaller boundary-layer region.

6. Approximate solution

In the previous section, the numerical solution for the developing boundary-layer flow ($x < x_0$) was sought and matched with the analytical solution for the fully developed viscous boundary-layer flow ($x > x_0$) at the transition point x_0 . In fact, the solution for the developing boundary-layer flow can be sought approximately using the Kármán–Pohlhausen momentum integral method, which has been used by Watson (1964) for the spread of a Newtonian jet along a flat plate. Owing to its relative simplicity and good accuracy, this method can be interesting and insightful, allowing direct comparison with the (exact) numerical solution for the spreading of a non-Newtonian jet along a flat plate. This will help to assess the range of validity and

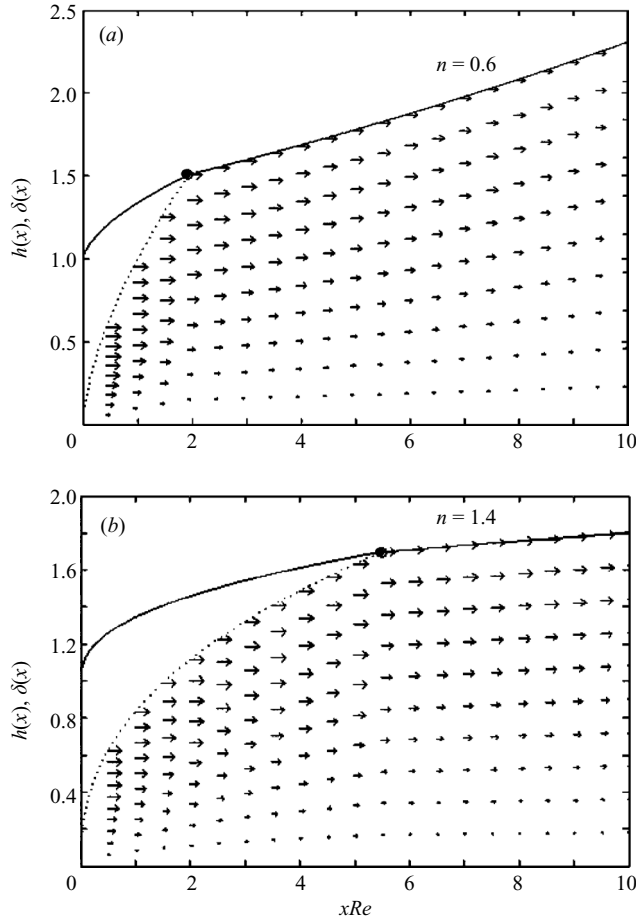


FIGURE 16. Streamwise velocity distribution for typical shear-thinning (a) and shear-thickening (b) fluids. Also shown are the free surface and boundary-layer limit. Note that the velocity magnitude in the boundary-layer region is equal to one. Solid circles show location of the transition point.

accuracy of the approximate procedure for non-Newtonian jets. Following Watson (1964), the approximate solution is sought by first assuming that the velocity profile at the transition point x_0 retains the same form (3.3) as for $x > x_0$. Thus, let

$$u(x < x_0, y) = f(\eta) \quad \text{with } \eta = y/\delta, \tag{6.1}$$

where $f(\eta)$ is governed by (3.7). In this case, the boundary-layer thickness is obtained by first integrating the momentum equation (2.5), or

$$\frac{d}{dx} \left[\int_0^\delta (u - u^2) dy \right] = (u_y)^n|_{y=0}. \tag{6.2}$$

Using (6.1) and (3.8), (6.2) leads to the following equation for $\delta(x < x_0)$:

$$\delta^n \delta' = K_n, \tag{6.3}$$

where $K_n = 3nc^{n+1}/(3nF_n - n - 1)$. Equation (6.3) is now integrated subject to the condition $\delta(x=0)=0$ to give

$$\delta(x \leq x_0) = [(n + 1)K_n x]^{1/(n+1)}. \tag{6.4}$$

When the position x_0 is reached, the boundary-layer absorbs all of the flow. In this case, $U(x = x_0) = 1$ and $h(x = x_0) = \delta(x = x_0)$. Hence, (3.10) leads to

$$\delta(x_0) = c/F_n, \tag{6.5}$$

which together with (6.4) gives the transition location, namely

$$x_0 = \frac{c^{n+1}}{(n + 1) K_n F_n^{n+1}}. \tag{6.6}$$

The volume flow rate is the sum of the flows inside and outside the boundary-layer, which gives

$$\delta \int_0^1 f(\eta) d\eta + h - \delta = 1. \tag{6.7}$$

The integral in (6.7) is determined from (3.8), and the film thickness in the developing layer becomes

$$h(x \leq x_0) = 1 + \left[1 - \frac{F_n}{c} \right] [(n + 1)K_n x]^{1/(n+1)}. \tag{6.8}$$

Finally, the integration constant l that appears in (3.11) and (3.12) can now be determined by recalling that $U(x = x_0) = 1$, and substituting x_0 from (6.6) into (3.11), namely

$$l \approx \frac{(n + 1)^2 K_n - 3n(2n - 1)c^{n+1}}{3n(n + 1)(2n - 1)K_n F_n^{n+1}}. \tag{6.9}$$

The shear stress at the plate defined by (3.15) now becomes

$$\tau_0(x < x_0) = \frac{[f'(0)]^n}{Re [(n + 1) K_n x]^{n/(n+1)}}. \tag{6.10}$$

In order to assess the accuracy of the above approximate solution, it is convenient to introduce the shear stress coefficient, which is defined as

$$C_n = \frac{\tau_0}{Re^{-1} x^{-n/(n+1)}} = \begin{cases} c^n [(n + 1)K_n]^{-n/(n+1)} & \text{(approximate),} \\ [\bar{f}''(0)]^n & \text{(numerical).} \end{cases} \tag{6.11a}$$

$$\tag{6.11b}$$

Here the approximate expression is obtained from (6.10) by using $f'(0) = c$, which is obtained from (3.8) at $\eta = 0$, while the numerical expression is obtained from (4.11). Figure 17 shows the dependence of C_n on the power-law index, n , and the comparison between the approximate and exact values as n is varied. There is generally good agreement between the two curves for moderately shear-thinning fluids and shear-thickening fluids. There is a growing discrepancy for strongly shear-thinning fluids as n decreases. Reasonable agreement is also consistent when other variables such as the film thickness, velocity at the free surface and shear stress at the plate are compared. However, as shown in figure 18, the approximate prediction for the velocity gradient $\bar{f}''(0)$ at the plate becomes generally inaccurate for shear-thinning fluids. This discrepancy has also been observed by Acrivos *et al.* (1960) in their study on the boundary-layer flow of power-law fluids along a flat plate, suggesting that the momentum integral method is not suitable for heat transfer calculations involving

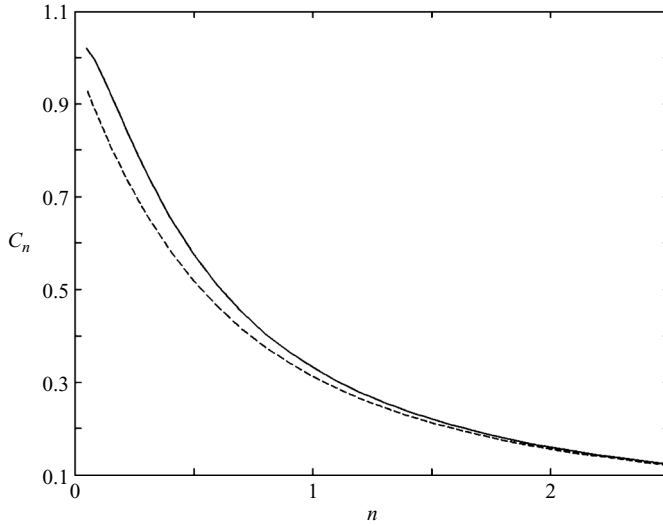


FIGURE 17. Dependence of the shear stress coefficient, C_n , on n , and comparison between the approximate (dashed curve) and numerical (solid curve) values.

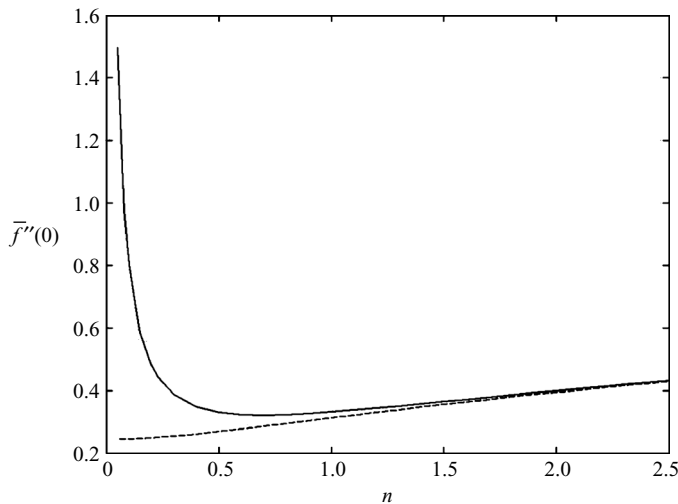


FIGURE 18. Dependence of the velocity gradient at the plate on n , and comparison between the approximate ($\bar{f}''(0) \approx (c_n)^{1/n}$, dashed curve) and numerical (solid curve) values.

non-Newtonian fluids since the velocity gradient $\bar{f}''(0)$ is the essential parameter in this case. In sum, the approximate solution appears to be reasonably accurate for the isothermal flow of practical non-Newtonian fluids. This is further confirmed when the results for the hydraulic jump are examined.

7. Hydraulic jump

In this section, the flow in the hydraulic jump region, region (iv), is considered for planar jumps. Following Watson (1964), the surface-tension effect is neglected, and the flow beyond the jump is assumed to be unidirectional. Consequently, flow

separation and the associate recirculation eddy are not considered. For circular jumps, the surface-tension effect is of radial and planar character, associated with the azimuthal curvature of the jump and the local curvature(s) in the plane of the jump, respectively. The flow structure in the vicinity of the jump depends on the jet strength or the distance of the jump from impingement. Two types of circular jump flow are usually identified in practice (Bush & Aristoff 2003). Type I jump, is of close proximity to impingement, and is thus marked by a jump of small radius and unidirectional flow at the surface, with boundary-layer separation beyond the jump. Type II jump, occurs farther from impingement, exhibiting reverse surface flow adjoining the jump, with wider radius and higher jump. Surface tension is shown to play a more significant role in Type I jumps as a result of the strong radial curvature. Surface tension is also expected to be important in Type II jumps as a result of the severe curvature at the nose and tail in the plane of the jump. Experiment, however, does not seem to suggest a prominent role for surface tension in this latter case (see the following).

In his theoretical development, Watson (1964) neglected the influence of surface tension, and assumed that the flow beyond the jump was unidirectional. Watson's theory appears to be adequate for the flow in the thin-film region. However, in the vicinity the hydraulic jump, the agreement has ranged from good to poor, being generally good when the jump radius is more than ten times the depth beyond the jump (Type II), and poor in the opposite limit of small jump radius (Type I). In their experimental study of water jumps, Liu & Lienhard (1993) observe that Watson's predictions are least satisfactory in the limit of a relatively weak jump, specifically when the ratio of the layer depths after and before the jump is small. Craik *et al.* (1981) focused on this small jump regime; their data for the jump radius thus underscored the shortcomings of Watson's theory. Bush & Aristoff (2003) revised Watson's predictions for the Type I jump by including only surface tension due to azimuthal curvature of the jump, and their predictions improved the agreement between experiment and theory, particularly in the weak-jump regime. In sum, the general consensus is that Watson's theory is reasonably accurate for Type II flow, despite the presence of severe curvature in the plane of the jump. This may be explained through the presence of strong separation at the jump tail, keeping the radial flow component essentially continuous, with the surface-tension effect being only local and far from the separation regions. Consequently, the present planar formulation and results can be regarded as adequate representation for large-radius circular jumps, even with the surface-tension effect neglected.

The position of the hydraulic jump, $x = x_j$, is determined by equating the rate of change of momentum to the force associated with the difference in pressure that arises from the elevation change. This assumption is legitimate provided that the width (measured in the streamwise direction) of the jump is small so that skin friction can be ignored. In this case, the dimensionless form for the condition of momentum is expressed as

$$\int_0^h u^2 dy - \int_0^H \bar{u}^2 dy = \frac{1}{Fr} \left(\int_0^H y dy - \int_0^h y dy \right) \approx \frac{H^2}{2Fr}. \quad (7.1)$$

Note that ρU_0^2 is taken as the pressure scale, and $Fr = U_0^2/ga$ is the Froude number at impingement, where g is the acceleration due to gravity. Here h and H are the depth on the inside and outside of the jump, respectively (see figure 1), and u and \bar{u} are the corresponding streamwise velocities. Owing to the complicated form of the expression

for h , it is undesirable to include the term $h^2/2Fr$, which is the pressure thrust on the inward side of the wave jump. This term, however, is only $O(h^2/H^2)$ compared with the thrust on the outward side. Also, the momentum outside the wave, which is $O(h/H)$ compared with that inside, will be included only approximately since it is assumed that the speed of flow \bar{u} immediately outside the jump is uniform, and therefore given by $\bar{u} = 1/H$ from the conservation of mass. In this case, (7.1) becomes

$$\frac{2Fr + H^3}{2HFr} = \int_0^h u^2 dy \quad (7.2)$$

It is necessary to evaluate the right-hand side of (7.2) separately for $x_j > x_0$ and for $x_j < x_0$, since the jump may occur at any point in the development of the boundary-layer. When $x_j \geq x_0$, the substitution of the similarity velocity profile (3.3) into (7.4) leads to

$$\frac{2Fr + H^3}{2HFr} = U^2 h \int_0^1 f^2(\eta) d\eta, \quad (7.3)$$

where the integral can be evaluated from (3.8), and then after using (3.11) and (3.12), (7.3) becomes

$$\frac{2Fr + H^3}{2HFr} = \left(\frac{x_j + l}{J_n} \right)^{1/(1-2n)}, \quad (7.4)$$

where $J_n = (n+1)^{2n} / ((3n)^{2n} (2n-1) F_n^{3n})$. Recall that l can be obtained numerically from (5.4) or approximately from (6.9). When $x_j < x_0$, the flow upstream of the jump consists of the developing boundary-layer and external inviscid flow, and must satisfy

$$\int_0^h u^2 dy = \int_0^\delta u^2 dy + h - \delta, \quad (7.5)$$

where u , h and δ are obtained numerically as in §5 or approximately as in §7. If the numerical solution is used, (7.2) and (7.5) give

$$\frac{2Fr + H^3}{2HFr} = \left(\int_0^{\eta_\delta} [\bar{f}'(\eta)]^2 d\eta - M_n \right) x_j^{1/(n+1)} + 1, \quad (7.6)$$

where $M_n = \eta_\delta F_n / c$, and the integral can be obtained by matching (7.6) with (7.4) at $x_j = x_0$. On the other hand, if the approximate solutions for u , h and δ are used, (7.5) becomes

$$\frac{2Fr + H^3}{2HFr} = N_n x_j^{1/(n+1)} + 1, \quad (7.7)$$

where $N_n = -(n+1)c^n [(n+1)K_n]^{-n/(n+1)}$. Figure 19 shows the influence of a non-Newtonian effect on the relation between the position of hydraulic jump $x_j Re$ and its height H . The influence of the Froude number can be incorporated if $(2Fr + H^3)/2HFr$ is plotted instead of H . It is shown that generally the hydraulic jump occurs earlier as the depth of flow downstream of the jump H increases. For both shear-thinning fluids (figure 19a) and shear-thickening fluids (figure 19b), the hydraulic jump occurs earlier when the flow is more viscous, experiencing more friction from the plate. In this case, the jet spreads with difficulty. In particular, figure 19(a) indicates that it is the level of viscosity and not the degree of shear thinning that dictates the position of the hydraulic jump (see also figure 12). This is in sharp contrast to the situation in figure 14(a) where shear thinning has a more drastic influence on the jet profile. Comparison between the numerical and approximate results is also shown in figure 19, which clearly hints to good agreement, confirming

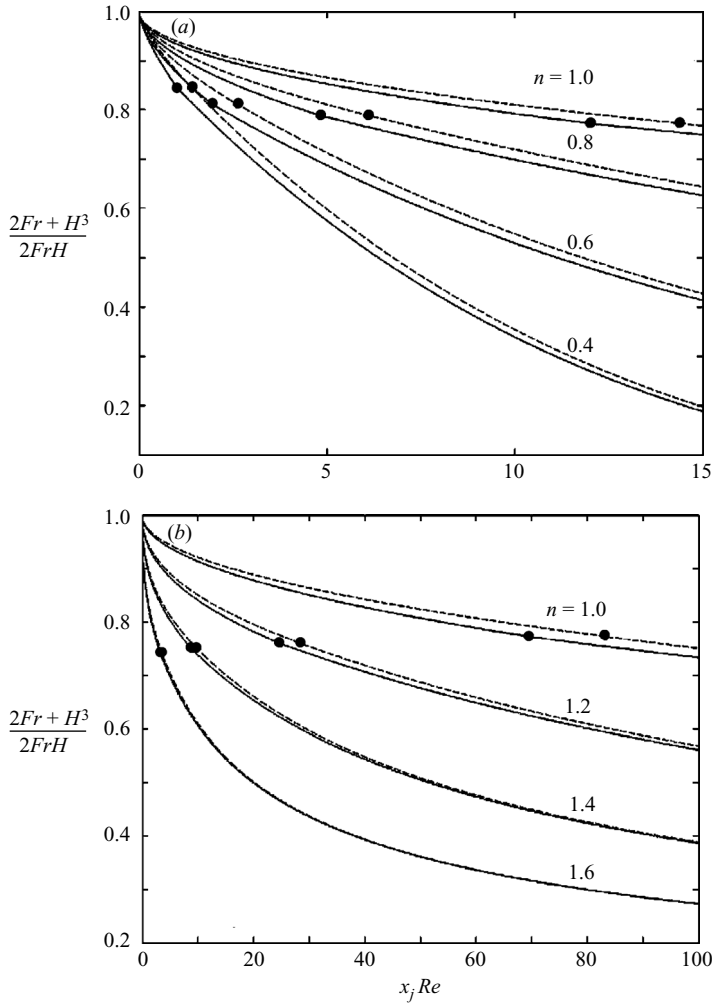


FIGURE 19. Dependence of jump height, H , on jump position, $x_j Re$, for (a) shear-thinning jets ($U_0 = 8 \text{ m s}^{-1}$), and (b) shear-thickening jets ($U_0 = 5 \text{ m s}^{-1}$). Here $a = 0.008 \text{ m}$ and $\rho = 998 \text{ kg m}^{-3}$. Comparison between exact (solid curves) and approximate (dashed curves) is shown, along with the position of the transition points (solid circles).

the earlier observation about the validity of the approximate approach for isothermal non-Newtonian spread.

8. Conclusion

This theoretical study focuses on the spread of a vertical non-Newtonian jet impinging on a solid flat plate. A hydraulic jump is assumed to form downstream from the impingement point. Both shear-thinning and shear-thickening fluids of the power-law type are considered. The flow domain is divided into three regions over the streamwise direction x , namely, a developing boundary-layer region (with potential upper layer), a fully developed viscous boundary-layer region (extending between the plate and free surface), and a hydraulic jump region.

In the fully developed viscous boundary-layer region, a similarity solution is obtained for both the free-surface velocity and film thickness, and the flow is shown to develop into a two-layer structure. The outer thin viscous layer is required to smooth out the singularity in viscosity at the free surface, allowing the inner algebraically decaying solutions to be matched smoothly with the solution near the free surface. Similarly, a similarity solution is sought numerically and approximately in the developing boundary-layer region. It is demonstrated that a viscous adjustment layer is required in order to ensure a smooth asymptotic matching to the far outer-field flow solution. The flow in the entire physical domain is obtained upon matching the flows between the developing and fully viscous boundary-layer regions.

Given the complex scaling used in the formulation, two real-fluid solutions are used to examine non-Newtonian effects, namely the shear-thinning xanthane and the shear-thickening ethylene in glycol, and simple fit of the experimental data allows the unambiguous interpretation of the results in terms of the power-law index n . Generally, the film thickness and shear stress at the plate increases and decreases, respectively, with x owing to resistance from the plate, at a rate that is stronger for the more viscous fluids. The growth of the boundary-layer thickness is commensurate with that of the free surface, but at a higher rate, whereas the shear stress decreases monotonically. For shear-thinning fluids, more viscous and strongly shear-thinning fluids spread with difficulty, even compared to highly viscous and simultaneously highly shear-thickening fluids. This illustrates the intricate flow behaviour resulting from the interplay between the shear-thinning character and the overall viscosity of the fluid. Comparison between the approximate and the numerical solutions shows generally good agreement, indicating that the approximate solution is reasonably accurate for the isothermal flow of practical non-Newtonian fluids. Finally, a relation is derived between the position and height of the hydraulic jump. Generally, the hydraulic jump is found to occur earlier as the depth of flow downstream of the jump increases. In contrast to the film profile and velocity, non-Newtonian effects seem to have little qualitative influence on the position of the hydraulic jump, which simply depends on the level of viscosity and not on the rate of shear-thinning or shear-thickening.

REFERENCES

- ACRIVOS, A., SHAH, M. & PETERSEN, E. E. 1960 Momentum and heat transfer in laminar boundary-layer flows of non-Newtonian fluids past external surface. *AIChE J.* **6**, 312–317.
- ANDERSSON, H. I. & IRGENS, F. 1988 Gravity-driven laminar film flow of power-law fluids along vertical walls. *J. Non-Newtonian Fluid Mech.* **27**, 153–172.
- BAONGA, J. B., LOUAHLIA-GUALOUS, H. & IMBERT, M. 2006 Experimental study of the hydrodynamic and heat transfer of free liquid jet impinging a flat circular heated disk, *Appl Thermal Engng'* **26**, 1125–1138.
- BEHRENS, R. A., CROCHET, M. J., DENSON, C. D. & METZNER, A. B. 1987 Transient free-surface flows: motion of a fluid advancing in a tube. *AIChE J.* **33**, 1178–1186.
- BIRD, R. B., STEWART, W. E. & LIGHTFOOT, E. N. 2002 *Transport Phenomena*. John Wiley.
- Brown, S. N. & Stewartson, K. 1965 On similarity solutions of the boundary-layer equations with algebraic decay. *J. Fluid Mech.* **23**, 673–678.
- BUSH, J. W. M. & ARISTOFF, J. M. 2003 The influence of surface tension on the circular hydraulic jump. *J. Fluid Mech.* **489**, 229–238.
- CHRISTANTI, Y. & WALKER, L. M. 2002 Effect of fluid relaxation time of dilute polymer solutions on jet breakup due to a forced disturbance. *J. Rheol.* **46**, 733–748.
- CRAIK, A., LATHAM, R., FAWKES, M. & GIBBON, P. 1981 The circular hydraulic jump. *J. Fluid Mech.* **112**, 347–362.

- DENIER, J. P. & DABROWSKI, P. P. 2004 On the boundary-layer equations for power-law fluids. *Proc. R. Soc. Lond. A*, **460**, 3143–3158.
- GORDON, M., YERUSHALMI, J. & SHINNAR, R. 1973 Instability of jets of non-Newtonian fluids. *Trans. Soc. Rheol.* **17**, 303.
- GOREN, S. L. & WRONSKI, S. 1966 The shape of low-speed capillary jets of Newtonian liquids. *J. Fluid Mech.* **25**, 185–198.
- GORLA, R. S. R. 1977 Laminar swirling power-law non-Newtonian fluid jet impinging on a normal plane. *J. Non-Newtonian Fluid Mech.* **2**, 299–306.
- GREEN, R. G. & GRISKEY, R. G. 1968 Rheological behaviour of dilatant (shear-thickening) fluids. Part I. Experimental and data. *Trans. Soc. Rheol.* **12**, 13–25.
- KASHKAROV, V. P. & MIKHAELIAN, B. M. 1973 Jets of a non-Newtonian fluid with a free surface. *Fluid Mech. Sov. Res.* **2**, 109–111.
- KHAYAT, R. E. & KIM, K. 2006 Thin-film flow of a viscoelastic fluid on an axisymmetric substrate of arbitrary shape. *J. Fluid Mech.* **552**, 37–71.
- KHAYAT, R. E. & WELKE, S. 2001 Influence of inertia, gravity and substrate topography on the two dimensional transient coating flow of a Newtonian fluid film. *Phys. Fluids* **13**, 355–367.
- KIM, K. & KHAYAT, R. E. 2002 Transient coating flow of a thin non-Newtonian fluid film. *Phys. Fluids* **14**, 2202–2215.
- LEE, J.-J. & MEI, C. C. 1996 Stationary waves on an inclined sheet of viscous fluid at high Reynolds and Weber numbers. *J. Fluid Mech.* **307**, 191–229.
- LEE, S. Y. & AMES, W. F. 1966 Similarity solutions for non-Newtonian fluids. *Am. Inst. Chem. Engrs J.* **6**, 700–708.
- LINDNER, A., BONN, D. & MEUNIER, J. 2000 Viscous fingering in a shear-thinning fluid. *Phys. Fluids* **12**, 256–261.
- LIU, X. & LIENHARD, J. 1993 The hydraulic jump in circular jet impingement and in other thin liquid films. *Exps. Fluids* **15**, 108–116.
- MIDDLEMAN, S. 1987 *Fundamental of Polymer Processing*. McGraw-Hill.
- OMODEL, B. J. 1979 Computer solutions of a plane Newtonian jet with surface tension. *Computers Fluids* **7**, 79.
- SARWESWAR, R. K. & MANOHAR, R. 1968 Stagnation point flows of non-Newtonian power-law fluids. *J. Appl. Maths* **19**, 84–88.
- SCHLICHTING, H. 1979 *Boundary-Layer Theory*. McGraw-Hill.
- SCHOWALTER, W. R. 1960 The application of boundary-layer theory to power-law pseudoplastic fluids: similar solutions. *Am. Inst. Chem. Engrs J.* **6**, 24–28.
- STEVENS, J. & WEBB, B. W. 1992 Measurements of the free surface flow structure under an impinging, free liquid jet. *Trans. ASME C: J. Heat Transfer* **114**, 79–84.
- WATSON, E. 1964 The spread of a liquid jet over a horizontal plane. *J. Fluid Mech.* **20**, 481–499.
- WEINSTEIN, S. J., RUSCHAK, K. J. & NG, K. C. 2003 Developing flow of a power-law liquid film on an inclined plane. *Phys. Fluids* **15**, 2973–2986.
- WU, J. & THOMPSON, M. C. 1996 Non-Newtonian shear-thinning flows past a flat plate. *J. Non-Newtonian Fluid Mech.* **66**, 127–144.